Article

Current Biology

Behavioral state-dependent modulation of insulin-producing cells in *Drosophila*

Graphical abstract

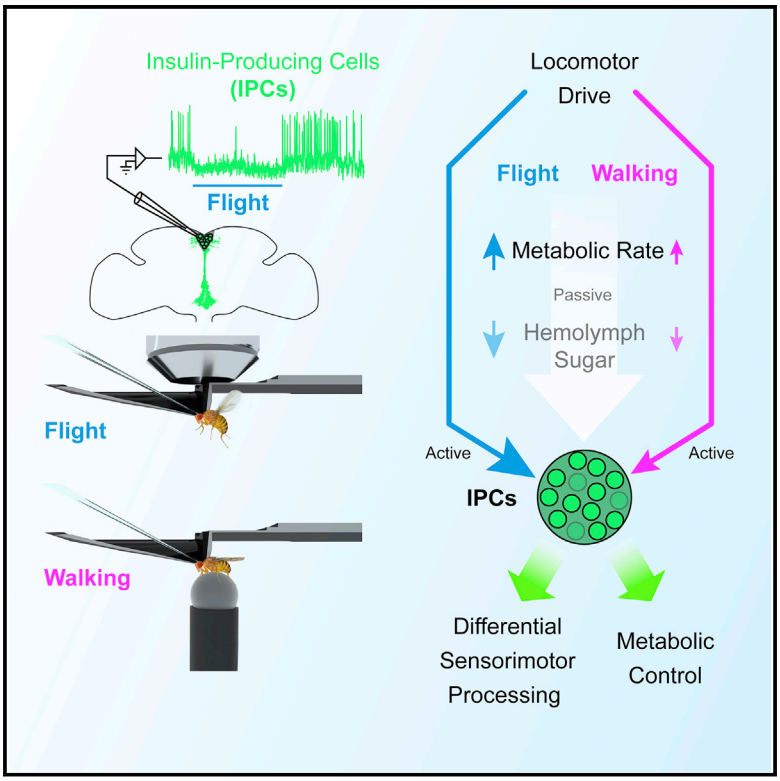

Authors

Sander Liessem, Martina Held, Rituja S. Bisen, Hannah Haberkern, Haluk Lacin, Till Bockemühl, Jan M. Ache

Correspondence

jan.ache@uni-wuerzburg.de

In brief

Liessem et al. show that the activity of insulin-producing cells is inhibited during locomotion and overshoots afterward. The inhibition is actively driven by neuronal pathways and stronger during metabolically more demanding flight than walking. This modulation serves to adjust the metabolic state to rapidly changing demands in behaving animals.

Highlights

- Insulin-producing cells (IPCs) are strongly and rapidly modulated by locomotion
- IPC activity is inhibited during and overshoots after cessation of locomotion
- IPC modulation is predictive of metabolic demands at behavioral transitions
- IPC inhibition is actively driven by feedforward neuronal pathways

Liessem et al., 2023, Current Biology *33*, 449–463
February 6, 2023
https://doi.org/10.1016/j.cub.2022.12.005

CellPress

Current Biology

CellPress

Article

Behavioral state-dependent modulation of insulin-producing cells in *Drosophila*

Sander Liessem,[1] Martina Held,[1] Rituja S. Bisen,[1] Hannah Haberkern,[2] Haluk Lacin,[3] Till Bockemühl,[4] and Jan M. Ache[1,5,6,*]

[1]Neurobiology and Genetics, Theodor-Boveri-Institute, Biocenter, Julius-Maximilians-University of Würzburg, Am Hubland, 97074 Würzburg, Germany

[2]HHMI Janelia Research Campus, 19700 Helix Drive, Ashburn, VA 20147, USA

[3]Department of Genetics, Washington University School of Medicine, 4523 Clayton Avenue, St Louis, MO 63110, USA

[4]Department of Biology, Institute of Zoology, University of Cologne, Zülpicher Str. 47b, 50674 Cologne, Germany

[5]Twitter: @Jan_Ache

[6]Lead contact

*Correspondence: jan.ache@uni-wuerzburg.de

https://doi.org/10.1016/j.cub.2022.12.005

SUMMARY

Insulin signaling plays a pivotal role in metabolic control and aging, and insulin accordingly is a key factor in several human diseases. Despite this importance, the *in vivo* activity dynamics of insulin-producing cells (IPCs) are poorly understood. Here, we characterized the effects of locomotion on the activity of IPCs in *Drosophila*. Using *in vivo* electrophysiology and calcium imaging, we found that IPCs were strongly inhibited during walking and flight and that their activity rebounded and overshot after cessation of locomotion. Moreover, IPC activity changed rapidly during behavioral transitions, revealing that IPCs are modulated on fast timescales in behaving animals. Optogenetic activation of locomotor networks *ex vivo*, in the absence of actual locomotion or changes in hemolymph sugar levels, was sufficient to inhibit IPCs. This demonstrates that the behavioral state-dependent inhibition of IPCs is actively controlled by neuronal pathways and is independent of changes in glucose concentration. By contrast, the overshoot in IPC activity after locomotion was absent *ex vivo* and after starvation, indicating that it was not purely driven by feedforward signals but additionally required feedback derived from changes in hemolymph sugar concentration. We hypothesize that IPC inhibition during locomotion supports mobilization of fuel stores during metabolically demanding behaviors, while the rebound in IPC activity after locomotion contributes to replenishing muscle glycogen stores. In addition, the rapid dynamics of IPC modulation support a potential role of insulin in the state-dependent modulation of sensorimotor processing.

INTRODUCTION

Insulin is central to an evolutionarily conserved signaling pathway controlling metabolic homeostasis in species ranging from nematodes and flies to mice and humans.[1–5] Accordingly, dysregulation of insulin signaling is a major cause for diseases like diabetes and obesity,[6] which in turn increase the risk of neurodegeneration and cognitive impairment.[7] Despite the importance of insulin signaling, the modulation of insulin release dynamics and the effects of insulin on the nervous system are not well understood. This is largely because insulin release and sensitivity depend on numerous internal and external variables.[8,9] Given the unparalleled genetic toolkit available in *Drosophila melanogaster*, flies can serve as a model system in which a detailed, mechanistic understanding of insulin signaling can be obtained *in vivo*. Since they also have a numerically smaller, less complex nervous system than mice or humans, the neuronal circuits and signaling pathways governing insulin release and the targets of insulinergic modulation can be identified and characterized more easily. Insulin-like peptides (ILPs) are expressed in a set of median neurosecretory cells in the pars intercerebralis (PI) of the insect brain, referred to as insulin-producing cells (IPCs).[10,11] Of the eight *Drosophila* ILPs (DILPs), IPCs express DILP2, 3, and 5 in adults.[12] Upon increased IPC activity, ILPs are released into the hemolymph,[11,13] the insect equivalent of blood,[14] via IPC axon terminals in the proventriculus, crop, aorta, and corpora cardiaca.[10,11,13,15–17] ILPs regulate circulating sugars,[12,18] which are mainly trehalose and glucose in insects.[19–22] In addition, insulin itself is a modulator of neuronal circuits controlling different aspects of food intake, metabolism, and behavior.[23–25] For example, locomotor activity is reduced when insulin levels are high, suggesting a general role of insulin in modulating sensorimotor pathways.[26] To date, most effects of insulin have been shown on slower and intermediate timescales. However, there is also evidence that insulin acts on sensorimotor pathways on faster timescales, for example, during predation[24] and escape behavior.[27,28]

Modulation of IPC activity and insulin release has been demonstrated in the context of feeding,[29–31] metabolism,[32,33]

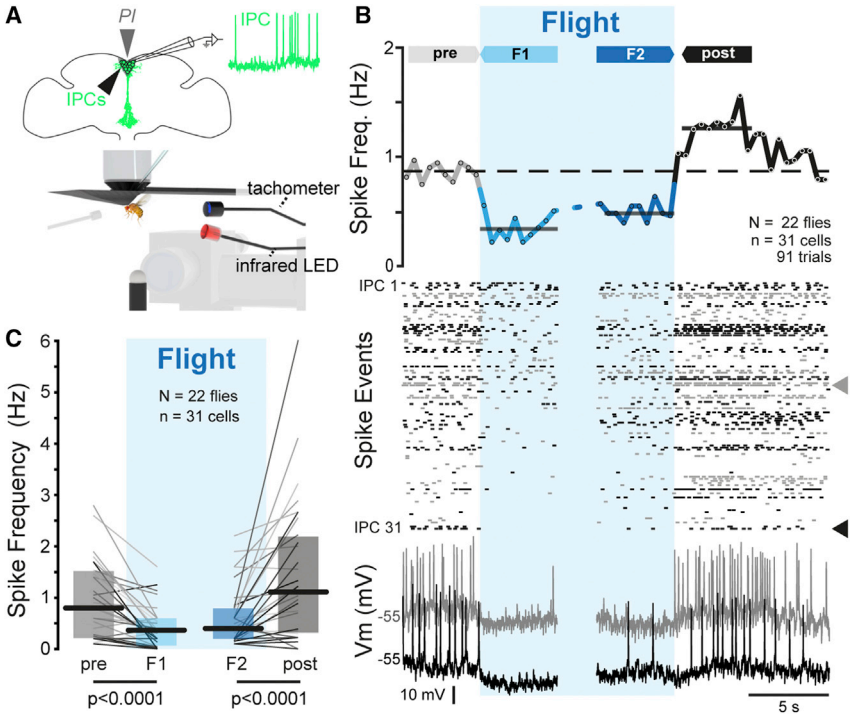

Figure 1. IPCs are inhibited during flight, and their activity rebounds and overshoots after flight cessation

(A) Schematic of experimental setup for *in vivo* recordings of IPCs during tethered flight. PI, pars intercerebralis. Tachometer was used to measure wingbeats.

(B) IPC activity in flight (blue shading). Top, mean IPC spike frequency (in 500-ms bins) across all trials. pre, F1, F2, and post indicate intervals for quantification in (C) (see STAR Methods). Dashed gray line, spike frequency before flight; solid lines, spike frequency in respective intervals. Middle, spike events from all trials. Bottom, two example recordings (arrowheads, corresponding spike event traces). Initial V_m of traces is indicated.

(C) Quantification of IPC responses (median ± IQR) based on trials in (B). Lines, mean responses of individual IPCs.

See also Figure S1 and Table S1.

nutrient sensing,[26,29,30,34] and circadian time.[35] Most of these experiments were carried out in *ex vivo* preparations[8,30,35–38] that did not permit animal behavior. Hence, even though the metabolic rate is dramatically increased during locomotion,[39–41] it is presently unclear whether IPC activity is modulated by the behavioral state. This question is particularly interesting in the context of insect flight, which is one of the most metabolically demanding processes in the animal kingdom.[42–44] Given the key role of insulin in governing metabolic homeostasis, modulation of IPC activity could adjust the metabolic rate in the context of locomotion. We therefore investigated whether IPC activity is modulated by the behavioral state, using *in vivo* patch-clamp recordings and calcium imaging in behaving *Drosophila*.

RESULTS

IPCs are inhibited during flight

Since metabolic demands are dramatically increased during locomotion, we hypothesized that IPC activity is modulated by locomotor state. To test this, we performed *in vivo* patch-clamp recordings from IPCs in *Drosophila* undergoing behavioral state transitions (Figure 1A). First, we quantified IPC activity before, during, and after flight. In particular, we analyzed IPC activity changes during the onset (first wingbeat) and cessation (last wingbeat) of flight. IPC activity was heavily affected by flight (Figure 1B). In suspended, resting animals, the baseline IPC spike frequency was 0.8 Hz (median, see Data S1 and Figure 1C), decreased significantly to 0.4 Hz at flight onset, and remained low throughout flight (F1 versus F2, $p > 0.1$). Interestingly, the spike frequency rebounded and overshot (from now on simplified as "rebound") relative to the pre-flight baseline after cessation of flight and stayed elevated for about 10 s at 1.1 Hz before returning to baseline (Figures 1B and 1C, pre versus post, $p < 0.05$). Hence, IPCs were strongly modulated by transitions into and out of flight.

Next, we asked whether the strength of IPC modulation was a function of flight performance. There was no strong correlation between the flight duration and the flight-dependent inhibition or rebound (Figures S1A and S1B). Since higher wingbeat frequencies require more energy, we also analyzed IPC activity changes as a function of wingbeat frequency. The average wingbeat frequency was 208 Hz, which is typical for tethered flight,[45,46] and there was no strong correlation between wingbeat frequency and IPC activity (Figures S1C and S1D). Hence, flight-dependent IPC modulation was robust and largely independent of flight duration and wingbeat frequency.

A small subset of IPCs was quiescent in the baseline condition and was therefore not considered in our initial analysis. To assess whether these IPCs were also modulated by flight, we depolarized them via current injection to induce spiking or increase spiking in spontaneously active neurons. Even when IPCs were depolarized, the flight-dependent inhibition was strong enough to significantly reduce spike rates across the IPC population (Figures S1E and S1F). In summary, IPC activity was strongly reduced during flight and rebounded after cessation of flight.

Flight modulates the IPC population activity

While the inhibition during flight was strong in the majority of IPCs, a subset of IPCs did not seem to be affected by flight in our patch-clamp experiments (Figures 1B and 1C). Since we were only able to record one IPC at a time, it was unclear whether this was due to heterogeneity within the IPC population activity. To investigate the flight-dependent modulation of IPCs simultaneously in multiple cells, we recorded the IPC population via widefield calcium imaging (Figure 2A). IPC somata were defined as regions of interest (ROIs; Figure 2B) and their $\Delta F/F$ values were aligned with flight behavior (Figure 2C; see STAR Methods). On average, we were able to image simultaneously from 9 out of the 14 IPCs (6–11 IPCs per fly, 71 total, N = 8 flies). We found

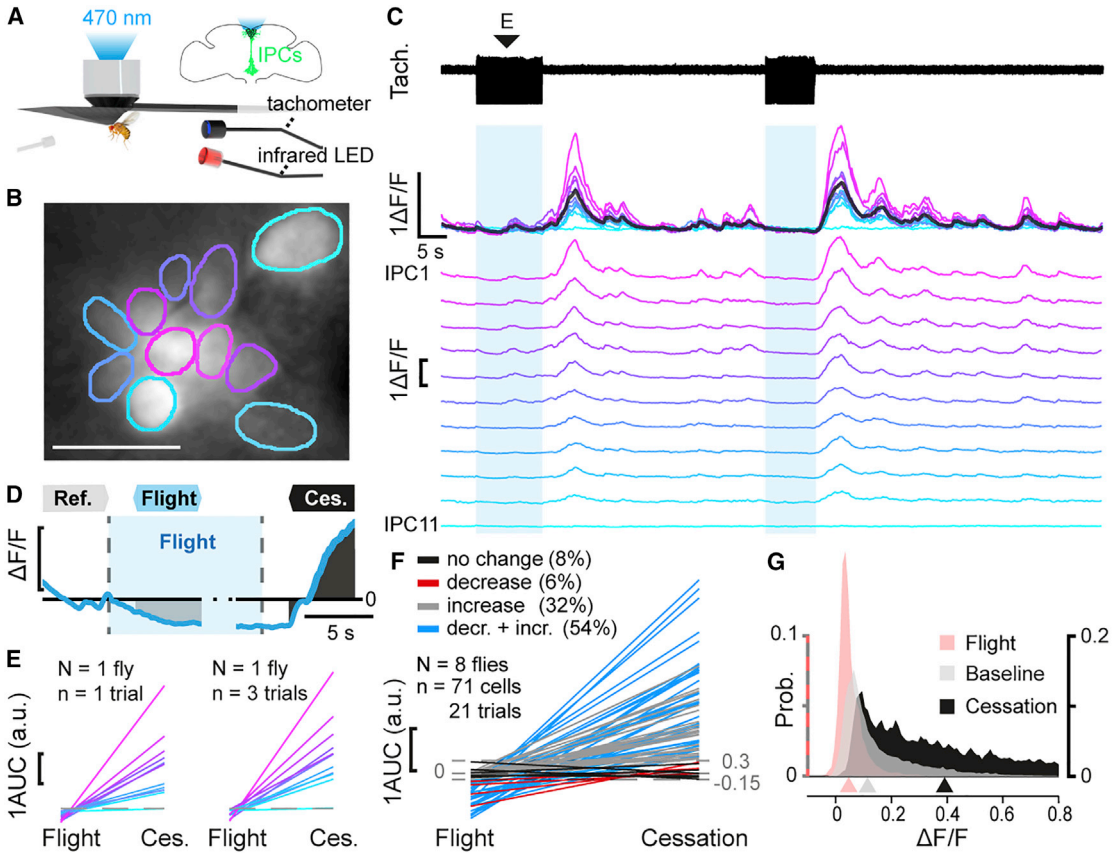

Figure 2. Calcium imaging reveals a flight-dependent modulation across the IPC population

(A) Experimental setup for imaging IPCs expressing GCaMP6m during flight.

(B) Example reference image of IPC somata as ROIs (color-coded as in C–E).

(C) Example traces of calcium responses during two subsequent flight bouts (blue shading). Top, wingbeat tachometer trace. Middle, ΔF/F of 11 IPCs and mean response (black). Bottom, individual ΔF/F responses.

(D) AUC calculation. Scale bars, 0.5 ΔF/F. Ref., baseline reference.

(E) AUC values of IPCs at flight onset and cessation. Left, responses from first flight trial in (C). Right, average response of 3 flight trials. Dashed line indicates zero.

(F) Average AUC at flight onset and cessation with color-coded response type based on lower (−0.15) and upper (0.3) AUC thresholds (gray).

(G) Probability distribution of ΔF/F values before (gray), during (red), and after flight (black, all in 0.01 ΔF/F bins). Arrowheads, median of each distribution. ΔF/F values above 0.8 are omitted.

See also Videos S1, S2, and S5 and Table S1.

a decrease in IPC fluorescence at flight onset and a dramatic increase after flight that exceeded the baseline activity (Figure 2C; see also Videos S1 and S2). Since the inhibitory effects seen in patch-clamp were less apparent in ΔF/F traces, we calculated their area under the curve (AUC; Figure 2D) and compared the probability distribution of ΔF/F values during different periods. The AUC was significantly higher after flight, compared with during flight, in individual flight trials, when averaged per IPC (Figure 2E), and across all flight trials ($p < 0.0001$, Figure 2F). The majority of IPCs exhibited both an inhibition at flight onset and a strong rebound at the cessation of flight (Figure 2F). However, 8% of IPCs did not show clear activity changes upon behavioral transitions, even though they occasionally exhibited spontaneous ΔF/F increases.

IPC inhibition during flight became even more apparent when comparing the probability distributions of ΔF/F values, with 93% of IPCs exhibiting a significant decrease at the onset of flight and 94% exhibiting a significant increase after flight cessation, compared with baseline ΔF/F levels (Figure 2G). Thus, although IPCs may be regarded as a functionally heterogeneous population,[47] the vast majority of IPCs display a strong, homogeneous response to locomotor state transitions.

IPCs are modulated by locomotor activity

Different modes of insect locomotion, such as flight and walking, use specific sets of muscles[48,49] that are controlled by two independent and fundamentally different motor systems with distinct neuronal organization in the brain and ventral nerve cord (VNC).[50] Moreover, metabolic rates increase from rest over walking to flight.[40,41,51] We therefore asked whether the modulation of IPC activity is a general feature across different locomotion modes or a specific adaptation to the high metabolic demands of flight. To test this, we recorded from IPCs in flies walking spontaneously on a spherical treadmill (Figure 3A). Based on individual walking trajectories, we distinguished between proper walking bouts (Figure 3) and bouts of less specific

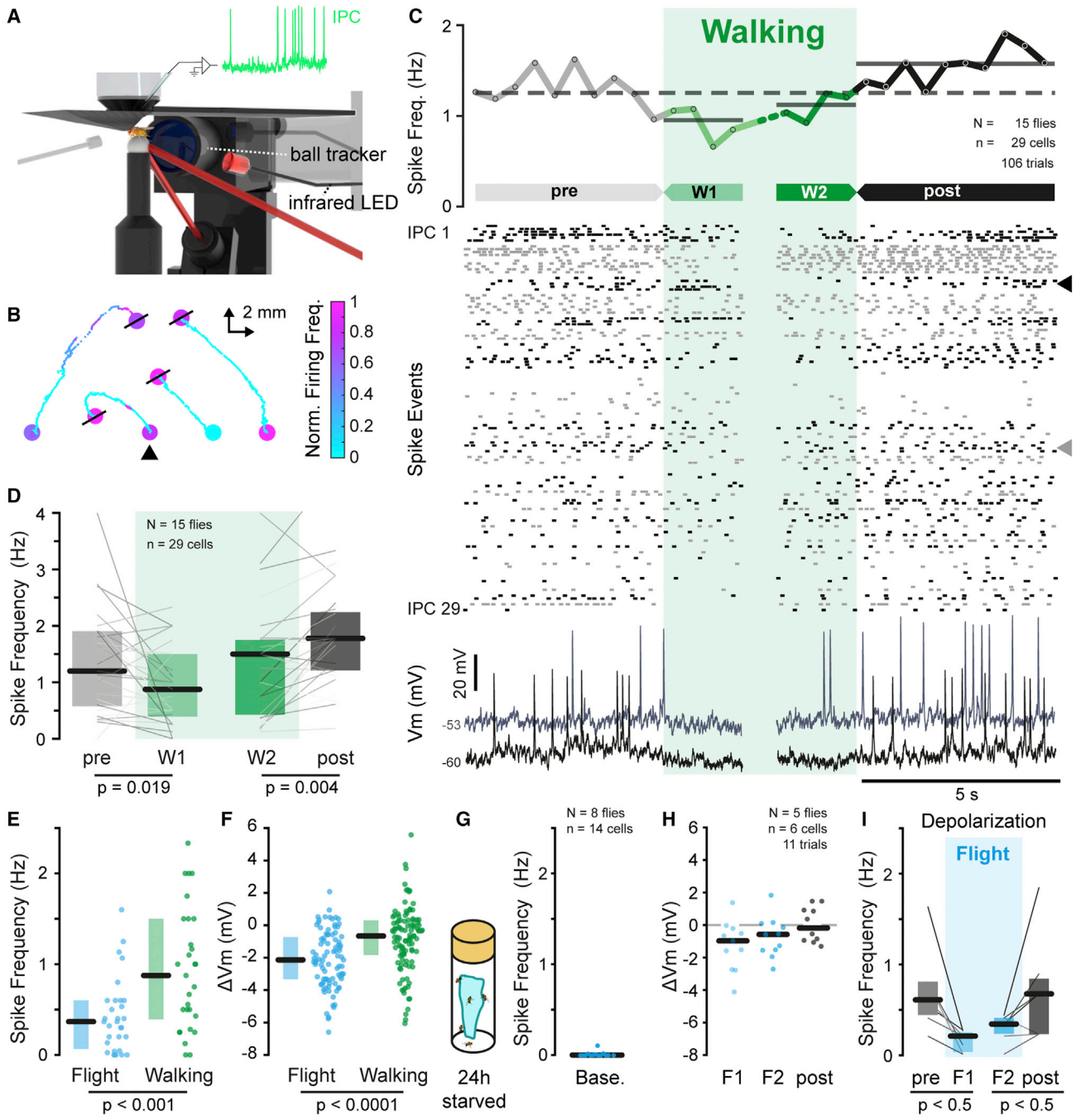

Figure 3. IPCs are modulated by walking, flight, and changes in metabolic state

(A) Experimental setup for *in vivo* patch-clamp recordings in walking flies.

(B) Representative walking trajectories with normalized IPC spike frequency (color-coded, binned as in C). Circles, start and final position of trajectory; black lines, walking cessation; arrowhead, black example shown in (C).

(C) IPC activity in walking flies (green shading). Top, mean IPC spike frequency (in 500-ms bins) averaged across all trials. pre, W1, W2, and post indicate intervals for quantification in (D). Dashed gray line, median spike frequency before walking; solid lines, median spike frequency in remaining intervals. Middle, spike events from all trials. Bottom, two example recordings (arrowheads). Initial V_m of traces is indicated.

(D) Quantification of IPC responses from trials in (B). One outlier at 4.8 Hz in post omitted for clarity of inspection. In (D)–(I), dots and thin lines indicate averages of individual IPCs, thick lines indicate population median, and boxplots IQR.

(E and F) Comparison of spike frequency (E) and V_m changes (F) during flight and walking.

(legend continued on next page)

locomotor activity (Figures S2A, S2C, and S2D; see STAR Methods). The effects of walking on IPC activity were similar to those of flight (Figures 3B–3D). Upon the onset of walking, the IPC spike frequency significantly decreased by 0.3 Hz, increased slightly during walking (W1 versus W2, $p < 0.05$), and rebounded to 1.8 Hz after cessation of walking (pre versus post, $p < 0.01$, Figure 3D). Even when all bouts of locomotor activity were included, the IPC modulation was apparent (Figures S2C and S2D). Combined with the strong flight-dependent modulation, these findings suggest that the modulation of IPCs is strongly coupled to locomotor activity in general.

Since metabolic rates increase with walking speed in insects,[39,52] we analyzed if IPC activity was modulated as a function of walking distance, speed, or duration (Figure S2). In our experiments, flies walked 14.8 mm at 1.7 mm/s, over 9 s on average, per walking bout. IPC modulation was largely independent of these parameters (Figure S2B; Data S1). Hence, the strength of IPC inhibition did not depend on the walking speed, suggesting it was not directly coupled to the metabolic rate of walking.

The difference in energy expenditure between walking speeds is likely small, compared with that between walking and flight. Hence, we investigated whether IPC modulation differed between walking and flight. Interestingly, IPC baseline activity was slightly but significantly higher in flies standing on the treadmill (1.2 Hz, Figure 3C), compared with flies without ground contact in periods between flight bouts (0.8 Hz, Figure 1C). Flies typically move their legs when they are neither standing nor flying (Video S3), which increases the metabolic rate.[53] These movements seemed to lead to a reduction in IPC activity similar to that observed during walking. Upon the onset of flight, IPC activity was further reduced to 0.4 Hz, which was less than half of the spike frequency during walking (0.9 Hz, Figure 3E). The hyperpolarization of the membrane potential (V_m) at the onset of flight was also significantly stronger, compared with the onset of walking (Figure 3F). Moreover, the spike frequency gradually increased during walking bouts (W1 versus W2, Figure 3D), which was not the case for flight. Hence, IPC inhibition was stronger during more energy-demanding flight, compared with less energy-demanding walking. This difference could either be explained by a larger number of IPCs being inhibited by flight than by walking or by stronger inhibition of individual IPCs. The number of non-modulated IPCs was similar during walking (7/29) and flight (6/31), and spike rates of individual IPCs were lower during flight compared with walking (Figures 3E and 3F). Therefore, the stronger inhibition of the IPC population during flight was driven by a stronger modulation of individual IPCs rather than the recruitment of additional IPCs.

Interactions between behavioral and metabolic state-dependent modulation of IPCs

Next, we asked whether IPC modulation during behavioral state transitions was comparable to effects of metabolic state changes known to affect insulin release. Starvation reduces DILP release from IPCs, as shown by immunofluorescence stainings,[54,55] so that we expected IPC activity to be low during starvation. To quantify this, we starved flies for 24 h and measured the IPC baseline spike frequency in glucose- and trehalose-free saline. Starvation abolished IPC spiking almost completely (Figure 3G). Hence, starvation had a stronger effect on IPC activity than flight, during which only about 25% of IPCs were completely quiescent (Figure 1C). However, both flight and starvation strongly inhibited IPCs and hence pulled their activity in the same direction.

Since IPC activity was affected both by metabolic and behavioral state changes, we next tested whether these two effects were interdependent. Spike frequencies were already approaching zero after starvation and were accordingly not further reduced during flight (Figure S2E). However, in starved flies, IPCs were significantly hyperpolarized at the onset of flight (Figure 3H, pre versus F1, $p < 0.0001$). Hence, IPCs were still inhibited. To test whether this inhibition was strong enough to reduce IPC spike frequency during flight after starvation, we depolarized IPCs to initiate spiking and induced flight. IPC spike frequency was significantly reduced at flight onset, remained low throughout flight (Figure 3I, F1 versus F2, $p > 0.05$), and increased back to baseline after cessation of flight (F2 versus post). This activity pattern basically matched that of fed flies, illustrating that IPC inhibition was unaffected by the metabolic state. However, starved flies were missing the prominent rebound excitation (pre versus post, $p = 0.94$) observed in fed flies. Matching this observation, the IPC V_m was not depolarized, compared with baseline after cessation of flight (pre versus post, $p = 1$, Figure 3H), which was the case in fed flies (Figure S1G). In summary, the inhibition of IPCs during flight is present in fed and starved flies, which indicates that it is independent of changes in hemolymph sugar levels. The rebound in IPC activity after locomotion, by contrast, was absent in starved flies and therefore seems to require hemolymph sugars.

IPCs are inhibited during optogenetically induced backward walking

Mechanistically, the behavioral state-dependent modulation of IPCs could have different origins (Figure 4A). On the one hand, IPC activity could be reduced during locomotion due to a depletion of hemolymph sugar levels, which IPCs sense cell autonomously[37] and via modulatory neuronal inputs.[8,56–58] Thus, IPC modulation would be a passive effect driven by changes in glucose concentrations (Figure 4A). On the other hand, IPCs could be modulated by neuronal activity correlated with walking and flight, such as feedback or feedforward signals from central modulatory, sensory, or motor circuits. Thus, IPCs would be actively modulated to adjust their activity to metabolically demanding states.

To understand which mechanism drives the IPC modulation, we used optogenetics to actively induce behavioral state transitions. To this end, we used the MDN-1 split-Gal4 driver line[59] to optogenetically activate a single class of command-like descending neurons (moonwalker descending neurons, MDNs)

(G) IPC baseline spike frequency after starvation.
(H) Flight-dependent V_m changes after starvation.
(I) Spike frequency of depolarized IPCs during flight after starvation.
See also Figure S2, Video S3, and Table S1.

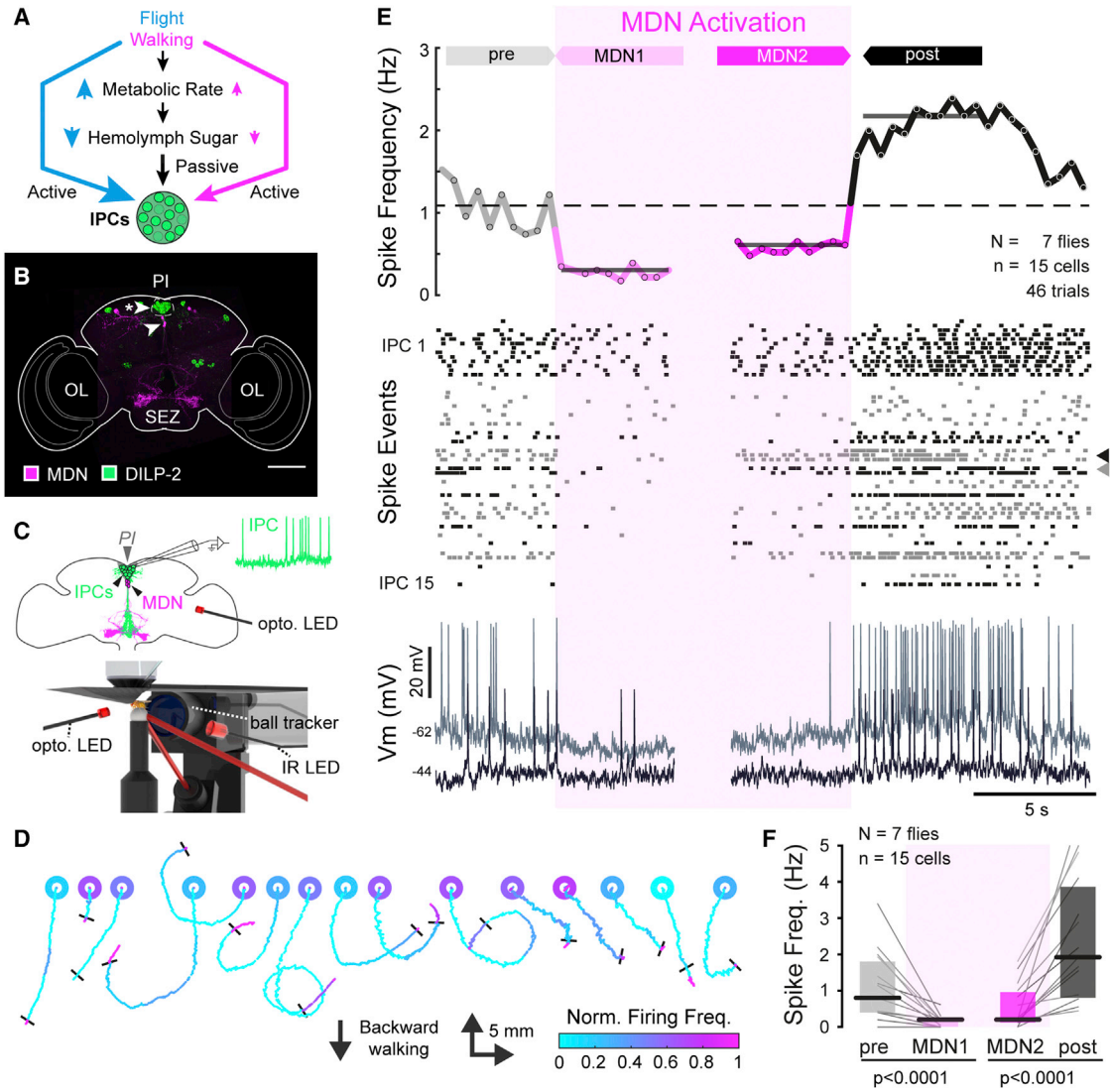

Figure 4. IPC activity is decreased during optogenetically induced backward walking

(A) Schematic showing locomotor effects on IPC activity.

(B) Confocal image of the central brain with MDNs and IPC labeling (see also Figures S3A–S3D).

(C) Experimental setup for patch-clamp recordings during optogenetically induced backward walking.

(D) Representative backward-walking trajectories with normalized IPC spike frequency (color-coded, binned as in E). Trajectories are plotted over 25 s (5 s pre, 15 s activation, and 5 s post). Circles, starting position (color, mean IPC spike frequency before MDN activation); black bar, cessation of activation.

(E) IPC activity during optogenetically induced backward walking. Plot details as in Figure 3C.

(F) Quantification of IPC responses from trials in (E). Plot details as in Figure 3D. One outlier at 6.8 Hz in post omitted for clarity of inspection.

See also Figure S3, Video S4, and Table S1.

and elicit backward walking (Figure 4B). We chose this line for several reasons (see STAR Methods). Most importantly, the primary outputs of MDNs are located close to the motor periphery in the VNC,[60] and activation of MDNs is sufficient to induce robust backward walking over tens of minutes.[59,60] Hence, activating MDNs provides an opportunity to directly control the animal's locomotor state while minimizing other effects on the central nervous system (CNS).

To test for effects of MDN activation on behavior and IPC activity, we recorded from IPCs in flies expressing the optogenetic effector CsChrimson[61] in MDN-1 (Figure 4C). Optogenetic activation of MDNs for 15 s induced robust and sustained backward walking (Figure 4D; Video S4). The IPC spike frequency decreased strongly at the onset of MDN activation, remained low throughout MDN activation (MDN1 versus MDN2, $p < 0.05$), and rebounded after cessation of MDN activation (Figures 4E and 4F, pre versus post, $p < 0.001$). These dynamics were similar to those observed during flight and forward walking.

Collectively, these findings support a model in which flight and walking, independent of whether it is spontaneous or elicited by optogenetically induced motor commands, modulate IPC activity in a similar fashion (Figure 4F). Interestingly, the IPC

modulation was much stronger during MDN activation than in spontaneously walking flies, even though MDN-induced backward walking was slower than forward walking. This indicates that behavioral state-dependent IPC modulation might be achieved actively, via a neuronal pathway, rather than passively, via changes in hemolymph sugar concentrations. Optogenetic stimulation of MDNs provides a strong drive to backward-walking motor circuits, which could explain the strong effects on IPCs during MDN-induced backward walking, despite the relatively low-level motor activity.

Modulation of IPCs precedes transitions in behavioral state

If the IPC inhibition was caused by locomotion-driven sensory feedback or changes in hemolymph sugar levels, it should arise after the behavioral onset. By contrast, if IPCs were modulated by a feedforward signal from motor centers, IPC inhibition should arise synchronously with, or even precede, locomotor activity (Figure 4A). To disambiguate between these possibilities and identify the mechanism responsible for IPC modulation, we analyzed the precise timing of IPC modulation. First, we quantified the change in V_m at flight onset and cessation. 1 s after the onset of flight, IPCs were significantly hyperpolarized by about 2.5 mV, compared with rest (Figure 5G, $p < 0.0001$). After cessation of flight, the V_m significantly increased by ~1 mV (Figure S1G, $p < 0.0001$) and was significantly higher than baseline ($p < 0.0001$), likely driving the rebound in spike frequency (Figures 1B and 1C). Interestingly, the decrease in V_m was already evident before flight onset in the grand average (Figures 5A and 5B) and individual example traces (Figure S4). Moreover, the V_m slowly returned toward baseline levels during flight, so that IPCs were significantly less hyperpolarized during the last seconds of flight, compared with the beginning (F1 versus F2, $p < 0.001$). In other words, IPCs were hyperpolarized just before the onset and started to depolarize before cessation of flight. Hence, changes in IPC V_m tended to precede behavioral transitions, suggesting that IPCs are actively modulated via a feedforward signal.

To further investigate the existence of a neuronal feedforward pathway, we quantified the timing of IPC inhibition relative to MDN activation and the onset of backward walking. To this end, we analyzed the IPC response to MDN activation (Figure 4) in two ways. First, we averaged the IPC V_m in a 2-s window around the onset of backward walking, as defined by the onset of treadmill rotations (Figure 5C). The average IPC membrane potential showed a clear and strong decrease just before the onset of walking, suggesting that the locomotor drive, rather than the actual locomotion or sensory feedback, was inhibiting IPCs. Next, we performed the same analysis but used the trigger of the LED driving MDN activation as the reference point for averaging (Figure 5D). Here, the V_m decreased much faster and reached a 0.6-mV-larger amplitude (−2 mV, Figure 5F). The time constant (τ) approximating the hyperpolarization was twice as fast (τ = 85 ms) when using the LED trigger, compared with actual walking (τ = 178 ms, Figure 5F). Hence, the variability of the decline in IPC V_m was much smaller when using the LED stimulus as the trigger, implying that MDN activation rather than the initiation of backward walking drove IPC inhibition. These results suggest that the inhibition of IPCs during locomotion is driven by a feedforward signal that precedes locomotor activity and changes in hemolymph sugar levels.

The behavioral state-dependent inhibition of IPCs is mediated by neuronal pathways

The timing of IPC activity changes suggested that a neuronal feedforward signal is responsible for the behavioral state-dependent IPC inhibition. To verify that IPCs are actively modulated via a neuronal pathway independent of sensory feedback and changes in sugar levels, we performed *ex vivo* recordings of IPCs while driving locomotor circuits via MDN activation and clamping the CNS to constant sugar levels (Figure 6A). Thus, we were able to optogenetically impose a motor command that induced a fictive locomotor state of the CNS, perhaps comparable to pharmacologically induced fictive motor output in other preparations,[62–66] which was (1) decoupled from changes in behavior, (2) devoid of sensory feedback, and (3) did not lead to changes in surrounding sugar levels. Using this preparation, we obtained similar results as during *in vivo* stimulation of MDNs. IPC frequencies were significantly reduced at the onset of MDN activation ($p < 0.05$) and remained inhibited throughout MDN stimulation (MDN1 versus MDN2, $p > 0.8$). Interestingly, IPCs did not exhibit the prominent rebound after MDN activation we observed *in vivo*. Instead, their spike frequency remained lower after MDN activation (pre versus post, $p > 0.5$, Figure 1B; see also Figures 2C, 3C, and 4E for comparison). Comparison of the baseline-subtracted spike frequency after cessation of MDN activation revealed that the spike frequency *in vivo* increased significantly, whereas the spike frequency *ex vivo* decreased significantly (Figure 6E). These findings suggest that the inhibition and rebound of IPC activity are independently regulated. The inhibition of IPCs is driven by feedforward signals that are present *ex vivo*, without sensory feedback or changes in hemolymph sugar concentrations. By contrast, the rebound in IPC activity must be driven by neuronal feedback, changes in hemolymph sugar levels, or intrinsic properties of IPCs. Various neuron types exhibit a cell-intrinsic post-inhibitory rebound (PIR), defined as a period of increased neuronal excitability and spiking following inhibition.[67–69] To test if a PIR could explain the increased spike frequency after cessation of locomotion, we injected hyperpolarizing currents into IPCs *in vivo* (Figures S5A–S5D). IPCs did not exhibit characteristic rebound potentials (Figure S5A), which typically occur within 100 ms after hyperpolarization.[68,70,71] On the contrary, IPC spike frequency was significantly lower after release from hyperpolarization (Figures S5B–S5D). The rebound after cessation of locomotion is therefore not an intrinsic property of IPCs. Since the rebound was also absent *ex vivo* and after starvation, it is likely driven by feedback pathways that require changes in hemolymph sugar concentration.

Taken together, our results suggest a model in which the inhibition and rebound of IPC activity are independently regulated. IPC inhibition is driven by a neuronal feedforward signal from motor centers that actively suppresses IPC activity during locomotion and is not simply a consequence of reduced hemolymph sugar levels or sensory feedback (Figure 6F). The rebound in IPC activity, by contrast, requires changes in hemolymph concentrations and is driven by feedback signals. This modulation in IPC activity is ideally suited to serve the increased metabolic demand during locomotion and the need to replenish glycogen stores after locomotion, and it could enable differential sensorimotor processing in different behavioral states.

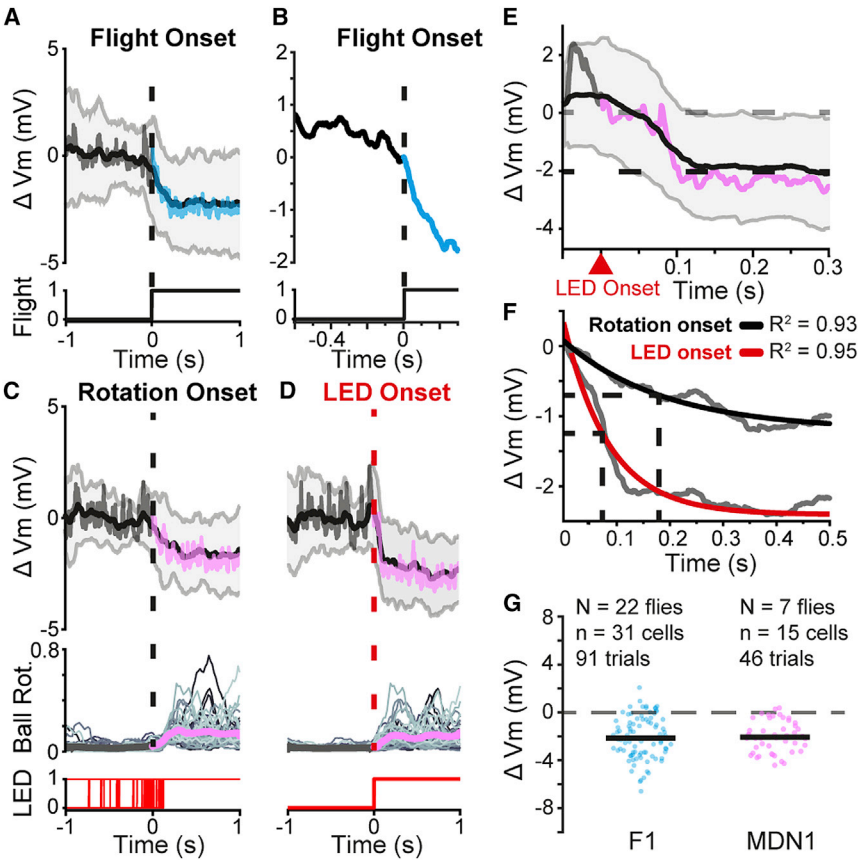

Figure 5. IPCs are rapidly inhibited at behavioral transitions

(A) Change in IPC V_m aligned to flight onset. Upper trace, mean V_m before (gray) and after (blue) flight onset. Black line, median-filtered V_m trace with SD (gray shading).

(B) Magnification of median-filtered V_m (A) at flight onset. The median filter follows the underlying change in V_m and does not change time course of the events (see Figure S4).

(C and D) Change in IPC V_m triggered by onset of treadmill rotation (C) and onset of LED (D). Top, mean V_m of IPCs before (gray) and after onset (magenta). Black line, median-filtered V_m with SD (gray shading). Middle, rectified ball rotation (a.u.) of all walking trials. Thick line, mean ball rotation. Bottom panels, LED onsets.

(E) Magnification of ΔV_m from (D). Black dashed line, mean median-filtered V_m. in MDN1.

(F) Average change in V_m aligned by the onset of LED and ball rotation with respective single exponential fits and R^2 values. Dashed lines, time constants (τ) for both averages.

(G) ΔV_m at flight (blue) and MDN stimulation onset (magenta). Dots, mean for each trial; black lines, median.

See also Figure S4 and Table S1.

DISCUSSION

Modulation of insulin release during locomotion is evolutionarily conserved

Since the role of insulin is highly conserved during evolution,[4,72–74] genetically tractable animal models such as *Drosophila* are powerful systems for studying aspects of insulin signaling, including those underlying human diseases such as obesity and diabetes.[75] Effects of physical exercise on circulating insulin levels are well described in vertebrates. However, how the activity of insulin-producing and -releasing cells is modulated to regulate insulin levels is still unclear. We set out to determine if and how IPCs are modulated by behavioral state transitions by leveraging the powerful genetic and physiological tools available in *Drosophila*.

We found a striking similarity in insulin regulation between humans and flies in situations where fuel stores need to be mobilized. IPCs, and hence likely the secretion of insulin, were inhibited at the onset of locomotion. Similar observations regarding the dynamics of insulin release were made in humans, where insulin levels are lower during excessive physical exercise.[76–79] This leads to the mobilization of fuel stores and the suppression of the fuel storage effects of insulin, thus shifting the metabolic balance toward a catabolic state. These fuel stores, particularly muscle glycogen, need to be replenished after physical activity, which is achieved through an enhanced sensitivity to insulin in depleted muscles.[80–82] We found that IPC activity in *Drosophila* rebounded and overshot at the cessation of locomotion, which could be a mechanism to rapidly replenish circulating insulin levels and stimulate glucose uptake and glycogen resynthesis in muscle and other tissues. The extent to which IPCs were modulated was tuned to the energy demands of ongoing behavior and was stronger in flight than in walking. Thus, behavioral state transitions have dramatic effects on IPC activity and hence insulin release, suggesting remarkable similarities in insulin signaling between flies and humans during increased physical activity.[77] These similarities offer the potential to study the effects of physical activity on metabolic control in disease models.[83–85]

Rapid IPC modulation ensures fuel availability in *Drosophila*

The regulation of fuel mobilization and metabolic fuels used to power insect flight (carbohydrates, lipids, or amino acids) differs between species and depends on dietary and behavioral specializations,[86–90] flight muscle types,[91,92] and the metabolic state.[93] Some of these differences might explain why IPC activity is tightly coupled to both the behavioral and nutritional states in *Drosophila*. Migratory locusts, as long-distance flyers, use trehalose as the main fuel in the initial phase of flight but switch to energy substrates from the fat body during sustained flight.[88,94] By contrast, other species, including *Drosophila*, primarily use carbohydrates to fuel flight.[86,93,95] Here, glycogen stores are heavily diminished in their major deposits after long periods of flight, while there is no reduction in the amount of stored fat.[93] This suggests that lipid metabolism only plays a minor role in powering *Drosophila* flight, underlining the importance of predictive insulin signaling to maintain hemolymph sugar homeostasis.

While the role of insulin is highly conserved, there are differences in the endocrinal regulation of energy mobilization

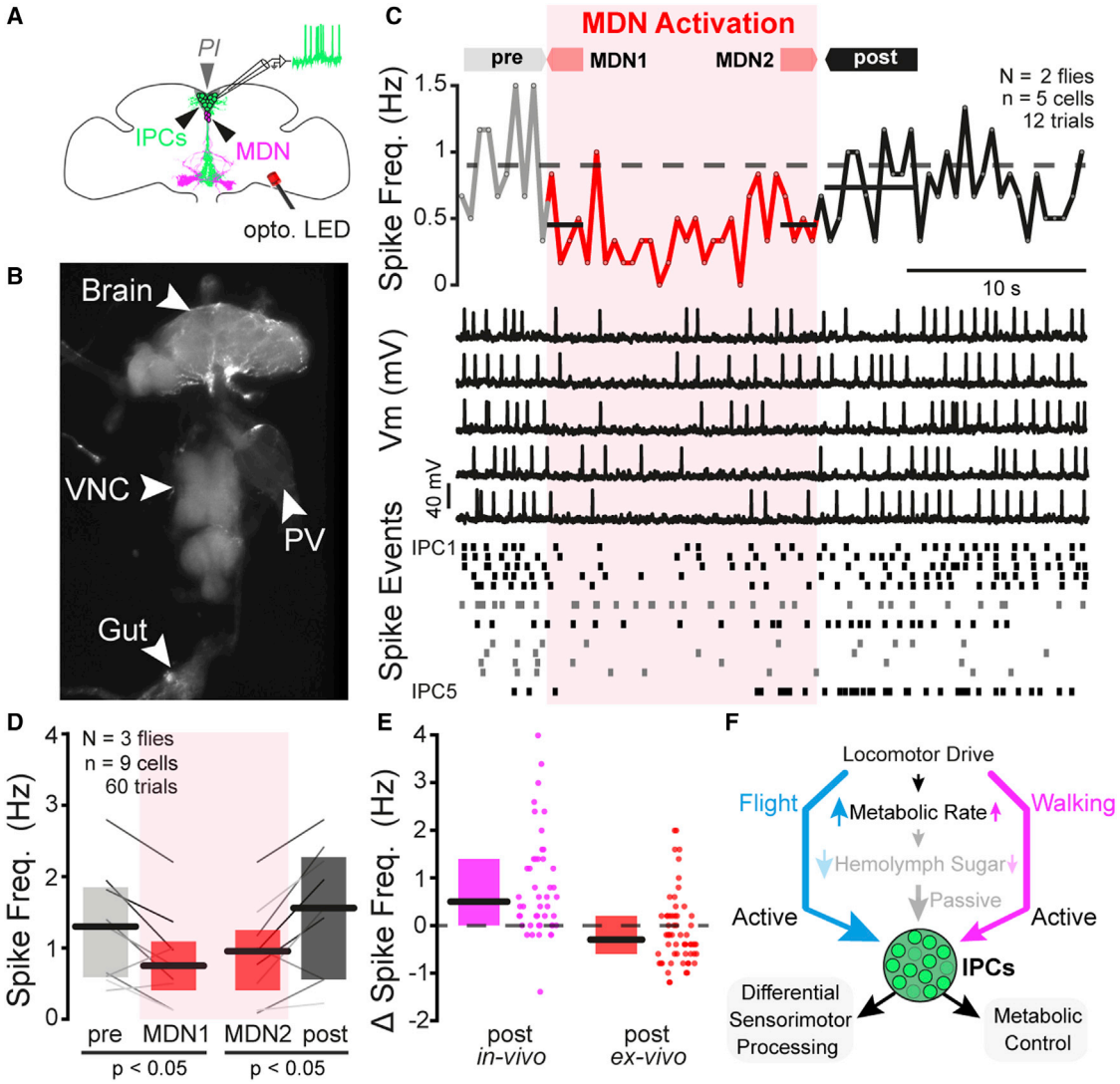

Figure 6. Optogenetic activation of MDN *ex vivo* shows that IPCs are inhibited by a neuronal pathway that actively suppresses IPC activity during locomotion

(A) Schematic illustrating *ex vivo* patch-clamp recordings from IPCs during optogenetic MDN activation.

(B) Dissected brain with attached VNC, proventriculus (PV), and gut.

(C) IPC activity during MDN activation (red shading) *ex vivo*. Top, mean IPC spike frequency (in 500-ms bins) across all trials. Gray dotted line, median spike frequency before MDN activation; solid black lines, median spike frequency in MDN1, MDN2, and post. Middle, five example trials from IPC1. Initial V_m was −47.4 mV (mean).

(D) IPC responses (median ± IQR) from trials in (C) and additional trials with 5-s LED stimulus. Lines indicate averages of individual IPCs.

(E) Change in spike frequency at cessation of the LED stimulus in *in vivo* and *ex vivo*. Dots, mean change in spike frequency for individual trials. Both distributions were significantly different from zero (two-sided Wilcoxon signed rank tests, $p < 0.0001$).

(F) Schematic summarizing the effects of walking and flight on the IPC population.

See also Figure S5 and Table S1.

between insects. Examples of neuromodulators promoting energy utilization are adipokinetic hormone/corazonin-related peptide (ACP)[96] and octopamine.[97–99] However, both ACP[96,100] and the octopaminergic neurons innervating insect flight muscles are absent in *Drosophila*.[101] Moreover, the role of octopamine in regulating hemolymph sugar levels in *Drosophila* is controversial,[102,103] and its effects on flight performance are more likely to be mediated through modulation of the CNS than via direct modulation of the metabolic state.[104] Most importantly, fuel switching in locusts[44,105] is mediated, inter alia, via release of adipokinetic hormone (AKH) into the hemolymph,[106–109] which promotes glycogenolysis through activation of glycogen phosphatase (GlyP)—the rate-limiting enzyme of glycogenolysis.[110] In *Drosophila*, by contrast, loss of AKH signaling does not seem to affect flight performance,[111] and AKH is unlikely to activate GlyP.[42] GlyP itself, however, is crucial for *Drosophila* flight performance[112] and is negatively regulated by DILP2.[113] Hence, a decrease in IPC activity and ultimately DILP2 release at flight

onset should increase GlyP activity, which in turn promotes the utilization of glycogen as the main fuel source.

There are situations in which both glycogen and fat body reserves are diminished in *Drosophila*, for example, starvation.[93] We show that in a state in which energy demands are high (flight) or glycogen and fat deposits are depleted (starvation), IPC activity is reduced. A causal link between IPC activity and hemolymph sugar homeostasis has been demonstrated by ablation of IPCs, which increases hemolymph sugar levels,[12,18] and overexpression of insulin, which reduces hemolymph sugar levels.[18] Moreover, insulin and hemolymph sugar levels increase after feeding,[54,114] where we measured high IPC activity, and decrease during starvation,[115,116] where we measured very low IPC activity. These observations highlight that our quantifications of IPC spike rates correlate with insulin release and that the magnitude of IPC modulation we measured is physiologically relevant in terms of modulating hemolymph sugar levels. Hence, the IPC spike frequency changes we observed during behavioral transitions are suited to modulate insulin release and hemolymph sugar levels in a predictive fashion. Accordingly, the rebound in IPC activity after cessation of locomotion was absent when glycogen stores were depleted (starvation) or physically removed (*ex vivo*). This could prevent a further decrease in hemolymph sugar levels (hypoglycemia/hypotrehalosemia) resulting from increased insulin release after locomotion. Together, these results underline the importance of integrating internal and behavioral states for the predictive and adaptive regulation of IPC activity.

Anticipatory IPC modulation sets the metabolic state during behavior

We hypothesized that IPC modulation could originate from intrinsic properties, feedback mechanisms, or feedforward mechanisms. Several of our findings suggest the presence of a feedforward mechanism. First, the hyperpolarization of the IPC membrane potential slightly preceded flight onset. Second, the IPC hyperpolarization was more strongly correlated with optogenetic activation of MDNs than actual behavior. Third, and most importantly, activation of MDNs in the absence of sensory feedback, muscles, actual behavior, and changes in surrounding sugar levels was sufficient to inhibit IPCs *ex vivo* (Figure 6). Hence, the inhibition of IPCs must be driven by feedforward signals. In humans and flies, anticipatory insulin release can be triggered by olfactory sensory cues signaling imminent food intake,[117,118] which prepare the body for incoming nutrients and thus prevent acute hyperglycemia.[119,120] In our model (Figure 6F), behavioral state-dependent IPC modulation primes the body for sudden changes in hemolymph sugar levels due to changes in metabolic demand at behavioral transitions. Interestingly, the rebound in IPC activity seems to rely on a feedback mechanism that depends on changes in hemolymph sugar levels: it was absent *ex vivo* and after starvation, and it is not mediated via PIR and hence not an intrinsic property of IPCs. IPCs can sense changes in glucose levels cell autonomously,[37] and indirectly via modulatory inputs from glucose-sensing neurons,[8,56,58] which could provide this feedback. The combination of feedback and feedforward mechanisms could improve the robustness of IPC modulation against perturbations, as suggested for other circuits requiring robust regulation.[121–123]

Which neurons relay the feedforward signal from the locomotor drive to IPCs? Given the relatively long latency between MDN activation and IPC inhibition (~90 ms, Figure 5), we assume that the connection between MDNs and IPCs is polysynaptic and the result of distributed feedback from motor circuits to modulatory circuits in the brain. In line with this, our initial exploration of the hemibrain EM volume[124,125] did not yield direct connections between MDNs and large, median neurosecretory cells in the PI, including the IPCs (which are not annotated yet due to their anatomical similarity to other neurons). Moreover, the primary output sites of MDNs are located in the VNC,[59] so that MDNs are very unlikely to make direct contacts with IPCs or other modulatory neurons in the brain. Instead, feedback from VNC motor circuits is most likely conveyed by ascending neurons, such as the moonwalker ascending neurons.[62] Given its ubiquitous role in modulating sensorimotor circuits across the CNS,[126–130] behavioral state dependence is likely mediated by a distributed network of neurons. For example, the neuronal pathways controlling flight and walking are fundamentally different,[50] but IPCs are inhibited during both, suggesting that different sensorimotor pathways converge to modulate IPCs. Since IPCs express a large variety of receptors for classical transmitters and neuropeptides,[33,47,55,131–134] their modulation might be achieved by a combination of various inputs, as shown in numerous other systems.[135–139] One candidate for mediating behavioral state-dependent IPC inhibition is GABA, which exerts a constant inhibitory tone on IPCs.[140]

Behavioral state-dependent modulation of sensorimotor pathways via insulin

One reason for an insect to take off or start walking is foraging. Although odors are dispersed and diluted by the ambient motion of air, flying insects can locate an odor source over tens of meters, which requires exquisite olfactory sensitivity. In *Drosophila*, olfactory sensitivity is modulated by the nutritional state,[34,141] which is partially mediated by insulin. Low levels of insulin in starved flies result in higher sNPF-receptor expression in specific odorant receptor neurons (ORNs), enhancing their sensitivity. The inhibition of IPCs during locomotion could be an elegant mechanism to simultaneously serve metabolic demands and aid the detection of food sources during locomotion,[142,143] since it should lead to ORN sensitization. ORN sensitization is achieved through changes in gene expression,[34] which require timescales exceeding the duration of a single flight or walking bout. However, *Drosophila* often display long series of locomotor events, for example, during the circadian activity peak or courtship,[144,145] and they can migrate over long distances for several hours.[146–148] Hence, the IPC inhibition during locomotion will lead to prolonged periods of low IPC activity on timescales sufficient to alter gene expression. Therefore, the behavioral state-dependent modulation of IPCs does not only serve metabolic demands but also potentially increases the success of finding food sources by tuning the sensitivity of the olfactory system during foraging. Insulin also modulates sensorimotor circuits on faster timescales, like those involved in escape behavior and pain responses.[27,28,149] Our results show that IPCs are modulated on equally fast timescales, demonstrating that insulin could play a role in rapidly shaping sensorimotor output.

Low insulin levels have protective effects against neurodegenerative disorders,[150,151] and impairment of insulin signaling extends lifespan in *Drosophila*,[12,152–154] *C. elegans*,[155,156] and mice.[157] This is partially because reduced insulin signaling promotes antioxidant defense, which in turn increases health and lifespan.[158] Our data suggest that high locomotor activity in *Drosophila* reduces insulin levels, which might explain why a physically active lifestyle increases lifespan and promotes healthy aging.

STAR★METHODS

Detailed methods are provided in the online version of this paper and include the following:

- KEY RESOURCES TABLE
- RESOURCE AVAILABILITY
  - Lead contact
  - Material availability
  - Data and code availability
- EXPERIMENTAL MODEL AND SUBJECT DETAILS
  - Fly husbandry
  - Fly stocks and genotypes
- METHOD DETAILS
  - Electrophysiology
  - Tethered flight and walking
  - Calcium imaging
  - Immunohistochemistry and image acquisition
- QUANTIFICATION AND STATISTICAL ANALYSIS

SUPPLEMENTAL INFORMATION

Supplemental information can be found online at https://doi.org/10.1016/j.cub.2022.12.005.

ACKNOWLEDGMENTS

This work was supported by a grant from the Deutsche Forschungsgemeinschaft to J.M.A. via the Emmy Noether program (DFG AC 371/1-1) and by a grant from the Deutsche Forschungsgemeinschaft to J.M.A. as part of the NSF/CIHR/DFG/FRQ/UKRI-MRC Next Generation Networks for Neuroscience (Neuronex) Program (DFG AC 371/2-1). T.B. is supported by Neuronex grant BU 857/15-1 from the Deutsche Forschungsgemeinschaft, and H.L. is supported by the National Institutes of Health grant NS122903. We thank Konrad Öchsner (Julius-Maximilians-Universität of Würzburg [JMU], Germany) and Michael Dübbert and Mehrdad Ghanbari (University of Cologne [UoC], Germany) for technical assistance; Charlotte Förster and Wolfgang Rössler (both JMU), Ansgar Büschges (UoC), Vivek Jayaraman (HHMI Janelia Research Campus, USA), and James W. Truman (Friday Harbor Laboratories, University of Washington, USA) for sharing resources; Jan A. Veenstra (University of Bordeaux, France) for providing the DILP-2 antibody; Dirk Rieger (JMU) for help setting up our lab in Würzburg; Christian Wegener and Meet Zandawala (both JMU) for comments on an earlier version of the manuscript; and Tanja Godenschwege (Florida Atlantic University, USA) for help with the *ex vivo* preparations and comments on an earlier version of the manuscript.

AUTHOR CONTRIBUTIONS

Conceptualization, S.L. and J.M.A.; experimental design, S.L. and J.M.A.; methodology, S.L., T.B., and J.M.A.; software, S.L., H.H., T.B., and J.M.A.; formal analysis, S.L., M.H., and J.M.A.; investigation, S.L., M.H., R.S.B., and J.M.A.; resources, H.L., T.B., and J.M.A.; writing – original draft, S.L. and J.M.A.; writing – review & editing, S.L., M.H., R.S.B., H.H., H.L., T.B., and J.M.A.; visualization, S.L., M.H., and J.M.A; supervision, J.M.A.; project administration, J.M.A; funding acquisition, J.M.A.

DECLARATION OF INTERESTS

The authors declare no competing interests.

INCLUSION AND DIVERSITY

One or more of the authors of this paper self-identifies as an underrepresented ethnic minority in their field of research or within their geographical location. One or more of the authors of this paper self-identifies as a gender minority in their field of research. One or more of the authors of this paper self-identifies as living with a disability. We support inclusive, diverse, and equitable conduct of research.

Received: June 23, 2022
Revised: November 1, 2022
Accepted: December 2, 2022
Published: December 28, 2022

REFERENCES

1. Partridge, L., Alic, N., Bjedov, I., and Piper, M.D. (2011). Ageing in *Drosophila*: the role of the insulin/Igf and TOR signalling network. Exp. Gerontol. *46*, 376–381.
2. Prentki, M., Matschinsky, F.M., and Madiraju, S.R. (2013). Metabolic signaling in fuel-induced insulin secretion. Cell Metab. *18*, 162–185.
3. Tatar, M., Bartke, A., and Antebi, A. (2003). The endocrine regulation of aging by insulin-like signals. Science *299*, 1346–1351.
4. Garofalo, R.S. (2002). Genetic analysis of insulin signaling in *Drosophila*. Trends Endocrinol. Metab. *13*, 156–162.
5. López-Otín, C., Blasco, M.A., Partridge, L., Serrano, M., and Kroemer, G. (2013). The hallmarks of aging. Cell *153*, 1194–1217.
6. Kahn, S.E., Hull, R.L., and Utzschneider, K.M. (2006). Mechanisms linking obesity to insulin resistance and type 2 diabetes. Nature *444*, 840–846.
7. Jais, A., Solas, M., Backes, H., Chaurasia, B., Kleinridders, A., Theurich, S., Mauer, J., Steculorum, S.M., Hampel, B., Goldau, J., et al. (2016). Myeloid-cell-derived VEGF maintains brain glucose uptake and limits cognitive impairment in obesity. Cell *165*, 882–895.
8. Oh, Y., Lai, J.S., Mills, H.J., Erdjument-Bromage, H., Giammarinaro, B., Saadipour, K., Wang, J.G., Abu, F., Neubert, T.A., and Suh, G.S.B. (2019). A glucose-sensing neuron pair regulates insulin and glucagon in *Drosophila*. Nature *574*, 559–564.
9. Ruud, J., Steculorum, S.M., and Brüning, J.C. (2017). Neuronal control of peripheral insulin sensitivity and glucose metabolism. Nat. Commun. *8*, 15259.
10. Cao, C., and Brown, M.R. (2001). Localization of an insulin-like peptide in brains of two flies. Cell Tissue Res. *304*, 317–321.
11. Nässel, D.R., and Vanden Broeck, J. (2016). Insulin/IGF signaling in *Drosophila* and other insects: factors that regulate production, release and post-release action of the insulin-like peptides. Cell. Mol. Life Sci. *73*, 271–290.
12. Broughton, S.J., Piper, M.D., Ikeya, T., Bass, T.M., Jacobson, J., Driege, Y., Martinez, P., Hafen, E., Withers, D.J., Leevers, S.J., and Partridge, L. (2005). Longer lifespan, altered metabolism, and stress resistance in *Drosophila* from ablation of cells making insulin-like ligands. Proc. Natl. Acad. Sci. USA *102*, 3105–3110.
13. Rulifson, E.J., Kim, S.K., and Nusse, R. (2002). Ablation of insulin-producing neurons in flies: growth and diabetic phenotypes. Science *296*, 1118–1120.
14. Hillyer, J.F., and Pass, G. (2020). The insect circulatory system: structure, function, and evolution. Annu. Rev. Entomol. *65*, 121–143.
15. Brogiolo, W., Stocker, H., Ikeya, T., Rintelen, F., Fernandez, R., and Hafen, E. (2001). An evolutionarily conserved function of the *Drosophila* insulin receptor and insulin-like peptides in growth control. Curr. Biol. *11*, 213–221.

16. Ghosh, S., Leng, W., Wilsch-Bräuninger, M., Barrera-Velázquez, M., Léopold, P., and Eaton, S. (2022). A local insulin reservoir in *Drosophila* alpha cell homologs ensures developmental progression under nutrient shortage. Curr. Biol. *32*. 1788–1797.e5.
17. Nässel, D.R. (2012). Insulin-producing cells and their regulation in physiology and behavior of *Drosophila*. Can. J. Zool. *90*, 476–488.
18. Belgacem, Y.H., and Martin, J.R. (2006). Disruption of insulin pathways alters trehalose level and abolishes sexual dimorphism in locomotor activity in *Drosophila*. J. Neurobiol. *66*, 19–32.
19. Wyatt, G.R. (1961). The biochemistry of insect hemolymph. Annu. Rev. Entomol. *6*, 75–102.
20. Evans, D.R., and Dethier, V.G. (1957). The regulation of taste thresholds for sugars in the blowfly. J. Insect Physiol. *1*, 3–17.
21. Howden, G., and Kilby, B. (1956). Trehalose and trehalase in the locust. Chem. Ind. (Lond.), 1453–1454.
22. Wyatt, G., and Kalf, G. (1956). Trehalose in insects. Fed. Proc. *15*, 322.
23. Brüning, J.C., Gautam, D., Burks, D.J., Gillette, J., Schubert, M., Orban, P.C., Klein, R., Krone, W., Müller-Wieland, D., and Kahn, C.R. (2000). Role of brain insulin receptor in control of body weight and reproduction. Science *289*, 2122–2125.
24. Bertsch, D.J., Martin, J.P., Svenson, G.J., and Ritzmann, R.E. (2019). Predatory behavior changes with satiety or increased insulin levels in the praying mantis (*Tenodera sinensis*). J. Exp. Biol. *222*, jeb197673.
25. Chen, S.L., Liu, B.T., Lee, W.P., Liao, S.B., Deng, Y.B., Wu, C.L., Ho, S.M., Shen, B.X., Khoo, G.H., Shiu, W.C., et al. (2022). WAKE-mediated modulation of cVA perception via a hierarchical neuro-endocrine axis in Drosophila male-male courtship behaviour. Nat. Commun. *13*, 2518.
26. Yu, Y., Huang, R., Ye, J., Zhang, V., Wu, C., Cheng, G., Jia, J., and Wang, L. (2016). Regulation of starvation-induced hyperactivity by insulin and glucagon signaling in adult *Drosophila*. eLife *5*, e15693.
27. Imambocus, B.N., Zhou, F., Formozov, A., Wittich, A., Tenedini, F.M., Hu, C., Sauter, K., Macarenhas Varela, E., Herédia, F., Casimiro, A.P., et al. (2022). A neuropeptidergic circuit gates selective escape behavior of Drosophila larvae. Curr. Biol. *32*. 149–163.e8.
28. Augustin, H., McGourty, K., Allen, M.J., Madem, S.K., Adcott, J., Kerr, F., Wong, C.T., Vincent, A., Godenschwege, T., Boucrot, E., and Partridge, L. (2017). Reduced insulin signaling maintains electrical transmission in a neural circuit in aging flies. PLoS Biol. *15*, e2001655.
29. Lin, S., Senapati, B., and Tsao, C.H. (2019). Neural basis of hunger-driven behaviour in *Drosophila*. Open Biol. *9*, 180259.
30. Qi, W., Wang, G., and Wang, L. (2021). A novel satiety sensor detects circulating glucose and suppresses food consumption via insulin-producing cells in *Drosophila*. Cell Res. *31*, 580–588.
31. Yao, Z., and Scott, K. (2022). Serotonergic neurons translate taste detection into internal nutrient regulation. Neuron *110*. 1036–1050.e7.
32. Kim, J., and Neufeld, T.P. (2015). Dietary sugar promotes systemic TOR activation in *Drosophila* through AKH-dependent selective secretion of Dilp3. Nat. Commun. *6*, 6846.
33. Birse, R.T., Söderberg, J.A., Luo, J., Winther, A.M., and Nässel, D.R. (2011). Regulation of insulin-producing cells in the adult Drosophila brain via the tachykinin peptide receptor DTKR. J. Exp. Biol. *214*, 4201–4208.
34. Root, C.M., Ko, K.I., Jafari, A., and Wang, J.W. (2011). Presynaptic facilitation by neuropeptide signaling mediates odor-driven food search. Cell *145*, 133–144.
35. Barber, A.F., Erion, R., Holmes, T.C., and Sehgal, A. (2016). Circadian and feeding cues integrate to drive rhythms of physiology in Drosophila insulin-producing cells. Genes Dev. *30*, 2596–2606.
36. Barber, A.F., Fong, S.Y., Kolesnik, A., Fetchko, M., and Sehgal, A. (2021). Drosophila clock cells use multiple mechanisms to transmit time-of-day signals in the brain. Proc. Natl. Acad. Sci. USA *118*. e2019826118.
37. Kréneisz, O., Chen, X., Fridell, Y.W., and Mulkey, D.K. (2010). Glucose increases activity and Ca^{2+} in insulin-producing cells of adult *Drosophila*. NeuroReport *21*, 1116–1120.
38. Li, Q., and Gong, Z. (2015). Cold-sensing regulates *Drosophila* growth through insulin-producing cells. Nat. Commun. *6*, 10083.
39. Berrigan, D., and Partridge, L. (1997). Influence of temperature and activity on the metabolic rate of adult Drosophila melanogaster. Comp. Biochem. Physiol. A Physiol. *118*, 1301–1307.
40. Full, R.J. (1997). Invertebrate locomotor systems. Comprehensive Physiology (Oxford University Press), pp. 853–930.
41. Harrison, J.F., and Roberts, S.P. (2000). Flight respiration and energetics. Annu. Rev. Physiol. *62*, 179–205.
42. Bretscher, H., and O'Connor, M.B. (2020). The role of muscle in insect energy homeostasis. Front. Physiol. *11*, 580687.
43. Sacktor, B. (1976). Biochemical adaptations for flight in the insect. Biochem. Soc. Symp. 111–131.
44. Wegener, G. (1996). Flying insects: model systems in exercise physiology. Experientia *52*, 404–412.
45. Bartussek, J., Mutlu, A.K., Zapotocky, M., and Fry, S.N. (2013). Limit-cycle-based control of the myogenic wingbeat rhythm in the fruit fly *Drosophila*. J. R. Soc. Interface *10*, 20121013.
46. Zanker, J.M. (1990). The wing beat of *Drosophila melanogaster*. I. Kinematics. Phil. Trans. R. Soc. Lond. B *327*, 1–18.
47. Nässel, D.R., and Zandawala, M. (2020). Hormonal axes in *Drosophila*: regulation of hormone release and multiplicity of actions. Cell Tissue Res. *382*, 233–266.
48. Dobi, K.C., Schulman, V.K., and Baylies, M.K. (2015). Specification of the somatic musculature in *Drosophila Drosophila*. Wiley Interdiscip. Rev. Dev. Biol. *4*, 357–375.
49. Maqbool, T., Soler, C., Jagla, T., Daczewska, M., Lodha, N., Palliyil, S., VijayRaghavan, K., and Jagla, K. (2006). Shaping leg muscles in Drosophila: role of ladybird, a conserved regulator of appendicular myogenesis. PLoS One *1*, e122.
50. Namiki, S., Dickinson, M.H., Wong, A.M., Korff, W., and Card, G.M. (2018). The functional organization of descending sensory-motor pathways in *Drosophila*. eLife *7*, e34272.
51. Rothe, U., and Nachtigall, W. (1989). Flight of the honey bee. J. Comp. Physiol. B *158*, 739–749.
52. Lighton, J.R.B., and Feener, D.H. (1989). A comparison of energetics and ventilation of desert ants during voluntary and forced locomotion. Nature *342*, 174–175.
53. Gordon, J., and Masek, P. (2021). Excessive energy expenditure due to acute physical restraint disrupts *Drosophila* motivational feeding response. Sci. Rep. *11*, 24208.
54. Géminard, C., Rulifson, E.J., and Léopold, P. (2009). Remote control of insulin secretion by fat cells in *Drosophila*. Cell Metab. *10*, 199–207.
55. Enell, L.E., Kapan, N., Söderberg, J.A., Kahsai, L., and Nässel, D.R. (2010). Insulin signaling, lifespan and stress resistance are modulated by metabotropic GABA receptors on insulin producing cells in the brain of *Drosophila*. PLoS One *5*, e15780.
56. Dus, M., Lai, J.S., Gunapala, K.M., Min, S., Tayler, T.D., Hergarden, A.C., Geraud, E., Joseph, C.M., and Suh, G.S. (2015). Nutrient sensor in the brain directs the action of the brain-gut axis in *Drosophila*. Neuron *87*, 139–151.
57. Kapan, N., Lushchak, O.V., Luo, J., and Nässel, D.R. (2012). Identified peptidergic neurons in the *Drosophila* brain regulate insulin-producing cells, stress responses and metabolism by coexpressed short neuropeptide F and corazonin. Cell. Mol. Life Sci. *69*, 4051–4066.
58. Kim, S.K., and Rulifson, E.J. (2004). Conserved mechanisms of glucose sensing and regulation by *Drosophila corpora cardiaca* cells. Nature *431*, 316–320.
59. Bidaye, S.S., Machacek, C., Wu, Y., and Dickson, B.J. (2014). Neuronal control of *Drosophila* walking direction. Science *344*, 97–101.
60. Feng, K., Sen, R., Minegishi, R., Dübbert, M., Bockemühl, T., Büschges, A., and Dickson, B.J. (2020). Distributed control of motor circuits for backward walking in *Drosophila*. Nat. Commun. *11*, 6166.

61. Klapoetke, N.C., Murata, Y., Kim, S.S., Pulver, S.R., Birdsey-Benson, A., Cho, Y.K., Morimoto, T.K., Chuong, A.S., Carpenter, E.J., Tian, Z., et al. (2014). Independent optical excitation of distinct neural populations. Nat. Methods *11*, 338–346.

62. Bidaye, S.S., Bockemühl, T., and Büschges, A. (2018). Six-legged walking in insects: how CPGs, peripheral feedback, and descending signals generate coordinated and adaptive motor rhythms. J. Neurophysiol. *119*, 459–475.

63. Biró, Z., Hill, R.H., and Grillner, S. (2008). The activity of spinal commissural interneurons during fictive locomotion in the lamprey. J. Neurophysiol. *100*, 716–722.

64. Marder, E. (2012). Neuromodulation of neuronal circuits: back to the future. Neuron *76*, 1–11.

65. Pulver, S.R., Bayley, T.G., Taylor, A.L., Berni, J., Bate, M., and Hedwig, B. (2015). Imaging fictive locomotor patterns in larval *Drosophila*. J. Neurophysiol. *114*, 2564–2577.

66. Wenzel, B., and Hedwig, B. (1999). Neurochemical control of cricket stridulation revealed by pharmacological microinjections into the brain. J. Exp. Biol. *202*, 2203–2216.

67. Goaillard, J.M., Taylor, A.L., Pulver, S.R., and Marder, E. (2010). Slow and persistent postinhibitory rebound acts as an intrinsic short-term memory mechanism. J. Neurosci. *30*, 4687–4692.

68. Bertrand, S., and Cazalets, J.R. (1998). Postinhibitory rebound during locomotor-like activity in neonatal rat motoneurons in vitro. J. Neurophysiol. *79*, 342–351.

69. Hartline, D.K., and Gassie, D.V., Jr. (1979). Pattern generation in the lobster (Panulirus) stomatogastric ganglion. I. Pyloric neuron kinetics and synaptic interactions. Biol. Cybern. *33*, 209–222.

70. Angstadt, J.D., Grassmann, J.L., Theriault, K.M., and Levasseur, S.M. (2005). Mechanisms of postinhibitory rebound and its modulation by serotonin in excitatory swim motor neurons of the medicinal leech. J. Comp. Physiol. A Neuroethol. Sens. Neural Behav. Physiol. *191*, 715–732.

71. Harris-Warrick, R.M., Coniglio, L.M., Barazangi, N., Guckenheimer, J., and Gueron, S. (1995). Dopamine modulation of transient potassium current evokes phase shifts in a central pattern generator network. J. Neurosci. *15*, 342–358.

72. Barbieri, M., Bonafè, M., Franceschi, C., and Paolisso, G. (2003). Insulin/IGF-I-signaling pathway: an evolutionarily conserved mechanism of longevity from yeast to humans. Am. J. Physiol. Endocrinol. Metab. *285*, E1064–E1071.

73. Das, D., and Arur, S. (2017). Conserved insulin signaling in the regulation of oocyte growth, development, and maturation. Mol. Reprod. Dev. *84*, 444–459.

74. Semaniuk, U., Piskovatska, V., Strilbytska, O., Strutynska, T., Burdyliuk, N., Vaiserman, A., Bubalo, V., Storey, K.B., and Lushchak, O. (2021). Drosophila insulin-like peptides: from expression to functions - a review. Entomol. Exp. Appl. *169*, 195–208.

75. Liguori, F., Mascolo, E., and Vernì, F. (2021). The genetics of diabetes: what we can learn from *Drosophila*. Int. J. Mol. Sci. *22*.

76. Ahlborg, G., and Felig, P. (1982). Lactate and glucose exchange across the forearm, legs, and splanchnic bed during and after prolonged leg exercise. J. Clin. Invest. *69*, 45–54.

77. Franckson, J.R., Vanroux, R., Leclercq, R., Brunengraber, H., and Ooms, H.A. (1971). Labelled insulin catabolism and pancreatic responsiveness during long-term exercise in man. Horm. Metab. Res. *3*, 366–373.

78. Pruett, E.D. (1970). Plasma insulin concentrations during prolonged work at near maximal oxygen uptake. J. Appl. Physiol. *29*, 155–158.

79. Wolfe, R.R., Nadel, E.R., Shaw, J.H., Stephenson, L.A., and Wolfe, M.H. (1986). Role of changes in insulin and glucagon in glucose homeostasis in exercise. J. Clin. Invest. *77*, 900–907.

80. Biolo, G., Williams, B.D., Fleming, R.Y., and Wolfe, R.R. (1999). Insulin action on muscle protein kinetics and amino acid transport during recovery after resistance exercise. Diabetes *48*, 949–957.

81. Richter, E.A., Garetto, L.P., Goodman, M.N., and Ruderman, N.B. (1982). Muscle glucose metabolism following exercise in the rat: increased sensitivity to insulin. J. Clin. Invest. *69*, 785–793.

82. Richter, E.A., Sylow, L., and Hargreaves, M. (2021). Interactions between insulin and exercise. Biochem. J. *478*, 3827–3846.

83. Katewa, S.D., Demontis, F., Kolipinski, M., Hubbard, A., Gill, M.S., Perrimon, N., Melov, S., and Kapahi, P. (2012). Intramyocellular fatty-acid metabolism plays a critical role in mediating responses to dietary restriction in *Drosophila melanogaster*. Cell Metab. *16*, 97–103.

84. Watanabe, L.P., and Riddle, N.C. (2019). New opportunities: *Drosophila* as a model system for exercise research. J. Appl. Physiol. (1985) *127*, 482–490.

85. Wen, D.T., Zheng, L., Yang, F., Li, H.Z., and Hou, W.Q. (2018). Endurance exercise prevents high-fat-diet induced heart and mobility premature aging and dsir2 expression decline in aging *Drosophila*. Oncotarget *9*, 7298–7311.

86. Suarez, R.K., Darveau, C.A., Welch, K.C., Jr., O'Brien, D.M., Roubik, D.W., and Hochachka, P.W. (2005). Energy metabolism in orchid bee flight muscles: carbohydrate fuels all. J. Exp. Biol. *208*, 3573–3579.

87. Teulier, L., Weber, J.M., Crevier, J., and Darveau, C.A. (2016). Proline as a fuel for insect flight: enhancing carbohydrate oxidation in hymenopterans. Proc. Biol. Sci. *283*, 20160333.

88. Lorenz, M.W., Kellner, R., Völkl, W., Hoffmann, K.H., and Woodring, J. (2001). A comparative study on hypertrehalosaemic hormones in the Hymenoptera: sequence determination, physiological actions and biological significance. J. Insect Physiol. *47*, 563–571.

89. Hou, L., Guo, S., Ding, D., Du, B., and Wang, X. (2022). Neuroendocrinal and molecular basis of flight performance in locusts. Cell. Mol. Life Sci. *79*, 325.

90. Clements, A.N. (1955). The sources of energy for flight in mosquitoes. J. Exp. Biol. *32*, 547–554.

91. Becker, A., Schlöder, P., Steele, J.E., and Wegener, G. (1996). The regulation of trehalose metabolism in insects. Experientia *52*, 433–439.

92. Cao, T., and Jin, J.P. (2020). Evolution of flight muscle contractility and energetic efficiency. Front. Physiol. *11*, 1038.

93. Wigglesworth, V.B. (1949). The utilization of reserve substances in Drosophila during flight. J. Exp. Biol. *26*, 150–163.

94. van Marrewijk, W.J.A., van den Broek, A.T.M., and Beenakkers, A.M.T. (1980). Regulation of glycogenolysis in the locust fat body during flight. Insect Biochem. *10*, 675–679.

95. Chadwick, L.E. (1947). The respiratory quotient of *Drosophila* in flight. Biol. Bull. *93*, 229–239.

96. Hou, L., Guo, S., Wang, Y., Nie, X., Yang, P., Ding, D., Li, B., Kang, L., and Wang, X. (2021). Neuropeptide ACP facilitates lipid oxidation and utilization during long-term flight in locusts. eLife *10*, e65279.

97. Duch, C., and Pflüger, H.J. (1999). DUM neurons in locust flight: a model system for amine-mediated peripheral adjustments to the requirements of a central motor program. J. Comp. Physiol. A *184*, 489–499.

98. Orchard, I., Ramirez, J.M., and Lange, A.B. (1993). A multifunctional role for octopamine in locust flight. Annu. Rev. Entomol. *38*, 227–249.

99. Mentel, T., Duch, C., Stypa, H., Wegener, G., Müller, U., and Pflüger, H.J. (2003). Central modulatory neurons control fuel selection in flight muscle of migratory locust. J. Neurosci. *23*, 1109–1113.

100. Hansen, K.K., Stafflinger, E., Schneider, M., Hauser, F., Cazzamali, G., Williamson, M., Kollmann, M., Schachtner, J., and Grimmelikhuijzen, C.J. (2010). Discovery of a novel insect neuropeptide signaling system closely related to the insect adipokinetic hormone and corazonin hormonal systems. J. Biol. Chem. *285*, 10736–10747.

101. Bräunig, P., and Pflüger, H.J. (2001). The unpaired median neurons of insects. Advances in Insect Physiology*28* (Academic Press), pp. 185–266.

102. Damrau, C., Toshima, N., Tanimura, T., Brembs, B., and Colomb, J. (2017). Octopamine and tyramine contribute separately to the counter-regulatory response to sugar deficit in *Drosophila*. Front. Syst. Neurosci. *11*, 100.

103. Li, Y., Hoffmann, J., Li, Y., Stephano, F., Bruchhaus, I., Fink, C., and Roeder, T. (2016). Octopamine controls starvation resistance, life span and metabolic traits in *Drosophila*. Sci. Rep. *6*, 35359.

104. Brembs, B., Christiansen, F., Pflüger, H.J., and Duch, C. (2007). Flight initiation and maintenance deficits in flies with genetically altered biogenic amine levels. J. Neurosci. *27*, 11122–11131.

105. Worm, R.A.A., and Beenakkers, A.M.T. (1980). Regulation of substrate utilization in the flight muscle of the locust, Locusta migratoria, during flight. Insect Biochem. *10*, 53–59.

106. Van der Horst, D.J. (2003). Insect adipokinetic hormones: release and integration of flight energy metabolism. Comp. Biochem. Physiol. B Biochem. Mol. Biol. *136*, 217–226.

107. Van der Horst, D.J., Van Marrewijk, W.J., and Diederen, J.H. (2001). Adipokinetic hormones of insect: release, signal transduction, and responses. Int. Rev. Cytol. *211*, 179–240.

108. Vroemen, S.F., Van der Horst, D.J., and Van Marrewijk, W.J. (1998). New insights into adipokinetic hormone signaling. Mol. Cell. Endocrinol. *141*, 7–12.

109. Gäde, G., Hoffmann, K.H., and Spring, J.H. (1997). Hormonal regulation in insects: facts, gaps, and future directions. Physiol. Rev. *77*, 963–1032.

110. Chatterjee, N., and Perrimon, N. (2021). What fuels the fly: energy metabolism in *Drosophila* and its application to the study of obesity and diabetes. Sci. Adv. *7*, eabg4336.

111. Gáliková, M., Diesner, M., Klepsatel, P., Hehlert, P., Xu, Y., Bickmeyer, I., Predel, R., and Kühnlein, R.P. (2015). Energy homeostasis control in *Drosophila* adipokinetic hormone mutants. Genetics *201*, 665–683.

112. Eanes, W.F., Merritt, T.J., Flowers, J.M., Kumagai, S., Sezgin, E., and Zhu, C.T. (2006). Flux control and excess capacity in the enzymes of glycolysis and their relationship to flight metabolism in *Drosophila melanogaster*. Proc. Natl. Acad. Sci. USA *103*, 19413–19418.

113. Post, S., Karashchuk, G., Wade, J.D., Sajid, W., De Meyts, P., and Tatar, M. (2018). *Drosophila* insulin-like peptides DILP2 and DILP5 differentially stimulate cell signaling and glycogen phosphorylase to regulate longevity. Front. Endocrinol. *9*, 245.

114. Ugrankar, R., Theodoropoulos, P., Akdemir, F., Henne, W.M., and Graff, J.M. (2018). Circulating glucose levels inversely correlate with *Drosophila* larval feeding through insulin signaling and SLC5A11. Commun. Biol. *1*, 110.

115. Sudhakar, S.R., Pathak, H., Rehman, N., Fernandes, J., Vishnu, S., and Varghese, J. (2020). Insulin signalling elicits hunger-induced feeding in *Drosophila*. Dev. Biol. *459*, 87–99.

116. Yamada, T., Habara, O., Kubo, H., and Nishimura, T. (2018). Fat body glycogen serves as a metabolic safeguard for the maintenance of sugar levels in *Drosophila*. Development *145*, dev158865.

117. Lushchak, O.V., Carlsson, M.A., and Nässel, D.R. (2015). Food odors trigger an endocrine response that affects food ingestion and metabolism. Cell. Mol. Life Sci. *72*, 3143–3155.

118. Skvortsova, A., Veldhuijzen, D.S., Kloosterman, I.E.M., Pacheco-López, G., and Evers, A.W.M. (2021). Food anticipatory hormonal responses: a systematic review of animal and human studies. Neurosci. Biobehav. Rev. *126*, 447–464.

119. Storlien, L.H. (1985). The ventromedial hypothalamic area and the vagus are neural substrates for anticipatory insulin release. J. Auton. Nerv. Syst. *13*, 303–310.

120. Woods, S.C. (1991). The eating paradox: how we tolerate food. Psychol. Rev. *98*, 488–505.

121. Dampney, R.A. (2016). Central neural control of the cardiovascular system: current perspectives. Adv. Physiol. Educ. *40*, 283–296.

122. Mauss, A.S., Meier, M., Serbe, E., and Borst, A. (2014). optogenetic and pharmacologic dissection of feedforward inhibition in drosophila motion vision. J. Neurosci. *34*, 2254–2263.

123. Kuo, A.D. (2002). The relative roles of feedforward and feedback in the control of rhythmic movements. Mot. Control *6*, 129–145.

124. Plaza, S.M., Clements, J., Dolafi, T., Umayam, L., Neubarth, N.N., Scheffer, L.K., and Berg, S. (2022). neuPrint: an open access tool for EM connectomics. Front. Neuroinform. *16*, 896292.

125. Scheffer, L.K., Xu, C.S., Januszewski, M., Lu, Z., Takemura, S.Y., Hayworth, K.J., Huang, G.B., Shinomiya, K., Maitlin-Shepard, J., Berg, S., et al. (2020). A connectome and analysis of the adult Drosophila central brain. eLife *9*, e57443.

126. Ache, J.M., Namiki, S., Lee, A., Branson, K., and Card, G.M. (2019). State-dependent decoupling of sensory and motor circuits underlies behavioral flexibility in *Drosophila*. Nat. Neurosci. *22*, 1132–1139.

127. Zolin, A., Cohn, R., Pang, R., Siliciano, A.F., Fairhall, A.L., and Ruta, V. (2021). Context-dependent representations of movement in *Drosophila* dopaminergic reinforcement pathways. Nat. Neurosci. *24*, 1555–1566.

128. Longden, K.D., and Krapp, H.G. (2009). State-dependent performance of optic-flow processing interneurons. J. Neurophysiol. *102*, 3606–3618.

129. Maimon, G. (2011). Modulation of visual physiology by behavioral state in monkeys, mice, and flies. Curr. Opin. Neurobiol. *21*, 559–564.

130. Maimon, G., Straw, A.D., and Dickinson, M.H. (2010). Active flight increases the gain of visual motion processing in *Drosophila*. Nat. Neurosci. *13*, 393–399.

131. Luo, J., Becnel, J., Nichols, C.D., and Nässel, D.R. (2012). Insulin-producing cells in the brain of adult *Drosophila* are regulated by the serotonin 5-HT1A receptor. Cell. Mol. Life Sci. *69*, 471–484.

132. Yurgel, M.E., Kakad, P., Zandawala, M., Nässel, D.R., Godenschwege, T.A., and Keene, A.C. (2019). A single pair of leucokinin neurons are modulated by feeding state and regulate sleep-metabolism interactions. PLoS Biol. *17*, e2006409.

133. Zandawala, M., Yurgel, M.E., Texada, M.J., Liao, S., Rewitz, K.F., Keene, A.C., and Nässel, D.R. (2018). Modulation of *Drosophila* post-feeding physiology and behavior by the neuropeptide leucokinin. PLoS Genet. *14*, e1007767.

134. Lee, K.S., Kwon, O.Y., Lee, J.H., Kwon, K., Min, K.J., Jung, S.A., Kim, A.K., You, K.H., Tatar, M., and Yu, K. (2008). *Drosophila* short neuropeptide F signalling regulates growth by ERK-mediated insulin signalling. Nat. Cell Biol. *10*, 468–475.

135. Weiss, K.R., Březina, V., Cropper, E.C., Hooper, S.L., Miller, M.W., Probst, W.C., Vilim, F.S., and Kupfermann, I. (1992). Peptidergic co-transmission in *Aplysia*: functional implications for rhythmic behaviors. Experientia *48*, 456–463.

136. Cropper, E.C., Lloyd, P.E., Reed, W., Tenenbaum, R., Kupfermann, I., and Weiss, K.R. (1987). Multiple neuropeptides in cholinergic motor neurons of *Aplysia*: evidence for modulation intrinsic to the motor circuit. Proc. Natl. Acad. Sci. USA *84*, 3486–3490.

137. Cropper, E.C., Miller, M.W., Tenenbaum, R., Kolks, M.A., Kupfermann, I., and Weiss, K.R. (1988). Structure and action of buccalin: a modulatory neuropeptide localized to an identified small cardioactive peptide-containing cholinergic motor neuron of *Aplysia californica*. Proc. Natl. Acad. Sci. USA *85*, 6177–6181.

138. Tritsch, N.X., Granger, A.J., and Sabatini, B.L. (2016). Mechanisms and functions of GABA co-release. Nat. Rev. Neurosci. *17*, 139–145.

139. Nusbaum, M.P., Blitz, D.M., and Marder, E. (2017). Functional consequences of neuropeptide and small-molecule co-transmission. Nat. Rev. Neurosci. *18*, 389–403.

140. Rajan, A., and Perrimon, N. (2012). Drosophila cytokine unpaired 2 regulates physiological homeostasis by remotely controlling insulin secretion. Cell *151*, 123–137.

141. Ko, K.I., Root, C.M., Lindsay, S.A., Zaninovich, O.A., Shepherd, A.K., Wasserman, S.A., Kim, S.M., and Wang, J.W. (2015). Starvation promotes concerted modulation of appetitive olfactory behavior via parallel neuromodulatory circuits. eLife *4*, e08298.

142. Getahun, M.N., Thoma, M., Lavista-Llanos, S., Keesey, I., Fandino, R.A., Knaden, M., Wicher, D., Olsson, S.B., and Hansson, B.S. (2016). Intracellular regulation of the insect chemoreceptor complex impacts odour localization in flying insects. J. Exp. Biol. *219*, 3428–3438.

143. Missbach, C., Dweck, H.K., Vogel, H., Vilcinskas, A., Stensmyr, M.C., Hansson, B.S., and Grosse-Wilde, E. (2014). Evolution of insect olfactory receptors. eLife *3*, e02115.

144. Pauls, D., Selcho, M., Räderscheidt, J., Amatobi, K.M., Fekete, A., Krischke, M., Hermann-Luibl, C., Ozbek-Unal, A.G., Ehmann, N., Itskov, P.M., et al. (2021). Endocrine signals fine-tune daily activity patterns in Drosophila. Curr. Biol. *31*. 4076–4087.e5.

145. Vanin, S., Bhutani, S., Montelli, S., Menegazzi, P., Green, E.W., Pegoraro, M., Sandrelli, F., Costa, R., and Kyriacou, C.P. (2012). Unexpected features of *Drosophila* circadian behavioural rhythms under natural conditions. Nature *484*, 371–375.

146. Dickinson, M.H. (2014). Death Valley, *Drosophila*, and the Devonian toolkit. Annu. Rev. Entomol. *59*, 51–72.

147. Götz, K.G. (1987). Course-control, metabolism and wing interference during ultralong tethered flight in *Drosophila melanogaster*. J. Exp. Biol. *128*, 35–46.

148. Powell, J.R., and Dobzhansky, T. (1976). How far do flies fly? Am. Sci. *64*, 179–185.

149. Im, S.H., Patel, A.A., Cox, D.N., and Galko, M.J. (2018). *Drosophila* insulin receptor regulates the persistence of injury-induced nociceptive sensitization. Dis. Model. Mech. *11*, dmm034231.

150. El-Ami, T., Moll, L., Carvalhal Marques, F., Volovik, Y., Reuveni, H., and Cohen, E. (2014). A novel inhibitor of the insulin/IGF signaling pathway protects from age-onset, neurodegeneration-linked proteotoxicity. Aging Cell *13*, 165–174.

151. Killick, R., Scales, G., Leroy, K., Causevic, M., Hooper, C., Irvine, E.E., Choudhury, A.I., Drinkwater, L., Kerr, F., Al-Qassab, H., et al. (2009). Deletion of Irs2 reduces amyloid deposition and rescues behavioural deficits in APP transgenic mice. Biochem. Biophys. Res. Commun. *386*, 257–262.

152. Clancy, D.J., Gems, D., Harshman, L.G., Oldham, S., Stocker, H., Hafen, E., Leevers, S.J., and Partridge, L. (2001). Extension of life-span by loss of CHICO, a *Drosophila* insulin receptor substrate protein. Science *292*, 104–106.

153. Tatar, M., Kopelman, A., Epstein, D., Tu, M.P., Yin, C.M., and Garofalo, R.S. (2001). A mutant *Drosophila* insulin receptor homolog that extends life-span and impairs neuroendocrine function. Science *292*, 107–110.

154. Min, K.J., Yamamoto, R., Buch, S., Pankratz, M., and Tatar, M. (2008). *Drosophila* lifespan control by dietary restriction independent of insulin-like signaling. Aging Cell *7*, 199–206.

155. Barsyte, D., Lovejoy, D.A., and Lithgow, G.J. (2001). Longevity and heavy metal resistance in daf-2 and age-1 long-lived mutants of *Caenorhabditis elegans*. FASEB J. *15*, 627–634.

156. Murakami, S., and Johnson, T.E. (1996). A genetic pathway conferring life extension and resistance to UV stress in *Caenorhabditis elegans*. Genetics *143*, 1207–1218.

157. Richardson, A., Liu, F., Adamo, M.L., Van Remmen, H., and Nelson, J.F. (2004). The role of insulin and insulin-like growth factor-I in mammalian ageing. Best Pract. Res. Clin. Endocrinol. Metab. *18*, 393–406.

158. Zarse, K., Schmeisser, S., Groth, M., Priebe, S., Beuster, G., Kuhlow, D., Guthke, R., Platzer, M., Kahn, C.R., and Ristow, M. (2012). Impaired insulin/IGF1 signaling extends life span by promoting mitochondrial L-proline catabolism to induce a transient ROS signal. Cell Metab. *15*, 451–465.

159. Veenstra, J.A., Agricola, H.J., and Sellami, A. (2008). Regulatory peptides in fruit fly midgut. Cell Tissue Res. *334*, 499–516.

160. Chen, T.W., Wardill, T.J., Sun, Y., Pulver, S.R., Renninger, S.L., Baohan, A., Schreiter, E.R., Kerr, R.A., Orger, M.B., Jayaraman, V., et al. (2013). Ultrasensitive fluorescent proteins for imaging neuronal activity. Nature *499*, 295–300.

161. Wong, M.Y., Zhou, C., Shakiryanova, D., Lloyd, T.E., Deitcher, D.L., and Levitan, E.S. (2012). Neuropeptide delivery to synapses by long-range vesicle circulation and sporadic capture. Cell *148*, 1029–1038.

162. Edelstein, A.D., Tsuchida, M.A., Amodaj, N., Pinkard, H., Vale, R.D., and Stuurman, N. (2014). Advanced methods of microscope control using μManager software. J. Biol. Methods *1*, e10.

163. Groth, A.C., Fish, M., Nusse, R., and Calos, M.P. (2004). Construction of transgenic *Drosophila* by using the site-specific integrase from phage phiC31. Genetics *166*, 1775–1782.

164. Venken, K.J., He, Y., Hoskins, R.A., and Bellen, H.J. (2006). P[acman]: a BAC transgenic platform for targeted insertion of large DNA fragments in *D. melanogaster*. Science *314*, 1747–1751.

165. Pfeiffer, B.D., Jenett, A., Hammonds, A.S., Ngo, T.T., Misra, S., Murphy, C., Scully, A., Carlson, J.W., Wan, K.H., Laverty, T.R., et al. (2008). Tools for neuroanatomy and neurogenetics in *Drosophila*. Proc. Natl. Acad. Sci. USA *105*, 9715–9720.

166. Akerboom, J., Chen, T.W., Wardill, T.J., Tian, L., Marvin, J.S., Mutlu, S., Calderón, N.C., Esposti, F., Borghuis, B.G., Sun, X.R., et al. (2012). Optimization of a GCaMP calcium indicator for neural activity imaging. J. Neurosci. *32*, 13819–13840.

167. Gouwens, N.W., and Wilson, R.I. (2009). Signal propagation in *Drosophila* central neurons. J. Neurosci. *29*, 6239–6249.

168. Berendes, V., Zill, S.N., Büschges, A., and Bockemühl, T. (2016). Speed-dependent interplay between local pattern-generating activity and sensory signals during walking in *Drosophila*. J. Exp. Biol. *219*, 3781–3793.

169. Seelig, J.D., Chiappe, M.E., Lott, G.K., Dutta, A., Osborne, J.E., Reiser, M.B., and Jayaraman, V. (2010). Two-photon calcium imaging from head-fixed rdrosophila during optomotor walking behavior. Nat. Methods *7*, 535–540.

170. Seelig, J.D., and Jayaraman, V. (2015). Neural dynamics for landmark orientation and angular path integration. Nature *521*, 186–191.

171. Wagh, D.A., Rasse, T.M., Asan, E., Hofbauer, A., Schwenkert, I., Dürrbeck, H., Buchner, S., Dabauvalle, M.C., Schmidt, M., Qin, G., et al. (2006). Bruchpilot, a protein with homology to ELKS/CAST, is required for structural integrity and function of synaptic active zones in *Drosophila*. Neuron *49*, 833–844.

REAGENT or RESOURCE	SOURCE	IDENTIFIER
Antibodies		
AlexaFluor 488 goat anti-chicken IgY (H+L)	Thermo Fisher Scientific, Waltham, MA, USA	RRID: AB_2534096
AlexaFluor 555 goat anti-rabbit IgG (H+L)	Thermo Fisher Scientific	RRID: AB_2535850
AlexaFluor 647 goat anti-mouse IgG (H+L)	Thermo Fisher Scientific	RRID: AB_2535804
rabbit anti-DILP2	Veenstra et al., Bordeaux, France[159]	RRID: AB_2569969
mouse anti-nc82 (Bruchpilot C-terminal aa 1227-1740)	Buchner, E.; Universitätsklinikum Würzburg, Germany[170]	RRID: AB_2314866
chicken anti-GFP (ab13970)	abcam, Berlin, Germany	RRID: AB_300798
Chemicals, peptides, and recombinant proteins		
All-trans-retinal	Sigma-Aldrich, Steinheim, Germany	R2500
Vectashield Antifade Mounting Medium (H-1000)	Vector Laboratories, CA, USA	N/A
Deposited data		
Primary data	This paper	https://doi.org/10.6084/m9.figshare.21302931
Experimental models: Organisms/strains		
10xUAS-myr:GFP	Bloomington Drosophila Stock Center (BDSC)	RRID:BDSC_32197
Dilp2-Gal4/CyO	BDSC	RRID: BDSC_37516
R96A08-LexA-p65 at VK00037	This study	N/A
LexOp-Dilp2::GFP at VK0001	This study	N/A
20x-UAS-CsChrimson (attP2)	BDSC	RRID: BDSC_32197
13XLexAop2-IVS-GCaMP6m-p10 su(Hw)attP5	Chen et al.[160]	N/A
VT50660.p65AD at attp2)/TM3-Ser	Bidaye et al.[59]	N/A
VT44845.GAL4DBD(attp40)/CyO	Bidaye et al.[59]	N/A
Oligonucleotides		
Forward primer to amplify *Dilp2*-GFP fragment: *GCTCGAGCCAACTTAATCCATTTGATCG*	This study	N/A
Reverse primer to amplify *Dilp2*-GFP fragment: *GCGATTGTCTAGAAAAGCTTAAAGCAGAATA*	This study	N/A
Recombinant DNA		
pUAST-Dilp2-GFP	Wong et al.[161]	N/A
Software and algorithms		
Leica Application Suite X (LAS X)	Leica Microsystems, Wetzlar, Germany	RRID:SCR_013673
Napari graphical user interface	https://napari.org/stable/	https://zenodo.org/record/7276432
pCLAMP 11 Software Suite	Molecular Devices, LLC., CA, USA	RRID:SCR_011323
fly2p	This paper	https://github.com/hjmh/fly2p
MATLAB 2020b	MathWorks, MA, USA	RRID:SCR_001622
Adobe Illustrator	Adobe, San Jose, CA, USA	RRID:SCR_010279
Micro-Manager 2.0	Edelstein et al.[162]	https://doi.org/10.14440/jbm.2014.36

STAR★METHODS

KEY RESOURCES TABLE

RESOURCE AVAILABILITY

Lead contact

Further information and requests for resources and reagents should be directed to and will be fulfilled by the lead contact, Jan M. Ache (jan.ache@uni-wuerzburg.de).

Material availability

Newly generated fly lines are listed in the key resources table and are available from the lead contact upon request.

Data and code availability

Raw data reported in this study have been deposited and are publicly available as of the date of publication. DOIs are listed in the key resources table.

Original Python code that is part of the fly2p module has been deposited at GitHub and is publicly available as of the date of publication. DOIs are listed in the key resources table.

Microscopy data reported in this paper will be shared by the lead contact upon request.

Any additional information required to reanalyze the data reported in this paper is available from the lead contact upon request.

EXPERIMENTAL MODEL AND SUBJECT DETAILS

Fly husbandry

All *Drosophila melanogaster* stocks were maintained on standard fly food (cornmeal-agar-molasses medium) at 25°C and 60% relative humidity under a 12 h/12 h light/dark cycle. All experiments were conducted on mated females that were used 3-6 days after eclosion. For starvation experiments, flies were wet starved for 24 h in a vial that only contained a water-soaked filter paper. For optogenetic activation experiments, one-day-old flies were transferred onto standard fly food containing 300 μM all-trans-retinal (R2500, Sigma-Aldrich, Steinheim, Germany). These vials were kept in the dark until the flies were used for experiments.

Fly stocks and genotypes

The genotypes used in each figure are listed in Table S1. The following genotypes were used (see also key resources table): for *in-vivo* whole cell patch-clamp recordings, IPCs were visualized using w; 10xUAS-IVS-myr:GFP (Bloomington #32197) and w; Dilp2-GAL4 / Cyo; w (Bloomington #37516). For optogenetic activation of MDNs during IPC patch-clamp recordings, the following lines were constructed:

LexAop-dilp2-GFP

Dilp2-GFP fragment was amplified from pUAST-Dilp2-GFP[161] via PCR using a pair of primers (*GCTCGAGCCAACTTAATCCATTT GATCG* and *GCGATTGTCTAGAAAAGCTTAAAGCAGAATA*) and was cloned into pJFRC19-13XLexAop2-IVS-myr::GFP vector via XhoI and XbaI mediated directional cloning. The transgene was inserted into the *attP* landing site of VK0001 on 2nd by using the phiC31 mediated site-specific integration.[163,164] 96A08-LexA-p65: 96A08 fragment[165] in Pcr8-GWTOPO was shuttled to the vector - pBpLexA-p65Uw via Gateway® cloning (Invitrogen, Waltham, MA, USA). The transgene was integrated into VK00037 attP site on 2nd chromosome as mentioned above.

Finally, the following line was generated: R96A08-LexA-p65 on VK00037, LexAOp-Dilp2::GFP in VK0001; 20XUAS-IVS-CsChrimson.mVenus in attP2 which was crossed to MDN-1: w; VT44845.GAL4DBD(attp40)/CyO; VT50660.p65AD(attp2)/TM3-Ser.[59] This line was used for optogenetic activation of a single class of command-like descending neurons (MDNs) to induce behavioral state transitions. We chose this particular line for several reasons: First, activation of MDNs is sufficient to induce robust backward walking over tens of minutes.[59,60] Second, optogenetic activation of residual MDN terminals in the VNC drives backward walking even after decapitation, and hence in the absence of higher brain regions. This is particularly important due to the regulatory complexity of IPC signaling. Third, MDNs activate motor networks in the VNC and receive visual input from optic glomerulus neurons. Hence, they are directly implicated in a sensorimotor pathway controlling locomotion, rather than setting the motivational state of the animal, which could affect IPC activity independent of locomotion. Fourth, the targets of MDNs in the VNC are well-defined and are all close to the motor periphery.[60] Finally, in contrast to other lines (including other MDN lines), off-target labelling in MDN-1 is very sparse and the moonwalker ascending neuron is not labelled (Figures 4B and S3). Hence, optogenetically activating MDNs provides an opportunity to directly control the animal's locomotor state while minimizing other effects on the nervous system. Functionality of CsChrimson in MDNs was confirmed based on the initiation of backward walking when illuminated by a flashlight prior to experiments.

For calcium imaging experiments, we used the following compound line: R96A08-LexA-p65 at VK37, LexAOp-GCaMP6m at attP5.[166,160] For immunohistochemistry we used the stocks listed in Table S1 and key resources table and in the figure legends.

METHOD DETAILS

Electrophysiology

Patch-clamp recordings in behaving flies were performed under daylight conditions at room temperature (RT) as described previously.[126,130] In brief, flies were cold anesthetized at 4°C and mounted with their head and thorax fixed to a pyramid-shaped fly holder, which left the legs and wings free to allow for flight (see Figure 1A) and walking (see Figure 3A). For the flight experiments presented in Figures 1, 2, 3E–3I, and 5D–5F, front legs were amputated at the level of the coxa-trochanter joint and the remaining leg stumps and the proboscis were glued to the thorax using UV glue (Proformic C1001, VIKO UG, Munich, Germany) to reduce interference with recordings. In all other *in-vivo* experiments, all legs remained intact and only the proboscis was glued. On the posterior side of the head, a small window was cut into the cuticle, exposing the IPCs. For patch-clamp recordings in *ex-vivo* preparations, the brain with attached VNC, proventriculus (PV) and gut was dissected and placed on a poly L-Lysin coated slide (Figure 6). In all patch-clamp

experiments, IPCs were visualized under a customized fluorescence microscope based on the SliceScope (Scientifica, Uckfield, UK). Collagenase (0.5% in extracellular saline) was locally applied with a blunt patch-pipette to rupture the neural sheath surrounding the brain in a small region over the IPCs to render the IPC somata accessible. In fed flies, the brain was continuously perfused with carbogenated (95% O_2/5% CO_2) extracellular saline with the following composition: 103 mM NaCl, 3 mM KCl, 5 mM N-Tris (hydroxymethyl)methyl-2-aminoethane-sulfonic acid, 8 mM trehalose, 10 mM glucose, 26 mM $NaHCO_3$, 1 mM NaH_2PO_4, 1.5 mM $CaCl_2$ and 4 mM $MgCl_2$ (adjusted to 273–275 mOsm, pH 7.3).[167] In *ex-vivo* experiments the entire CNS was continuously perfused in a large volume of extracellular saline. In starvation experiments, fly brains were perfused with extracellular glucose free saline containing 103 mM NaCl, 3 mM KCl, 5 mM N-Tris (hydroxymethyl)methyl-2-aminoethane-sulfonic acid, 20 mM sucrose, 26 mM $NaHCO_3$, 1 mM NaH_2PO_4, 1.5 mM $CaCl_2$, 4 mM $MgCl_2$ (osmolarity adjusted to 273-275 mOsm, pH 7.3).

Patch-clamp electrodes (4-8 MΩ) containing intracellular saline (40 mM potassium aspartate, 10 mM HEPES, 1 mM EGTA, 4 mM MgATP, 0.5 mM Na_3 GTP, 1 mM KCl and 20 μM, adjusted to 260–275 mOsm, pH 7.3) were used for whole cell patch-clamp experiments. Intracellular traces were recorded with the pCLAMP 11 Software Suite (Molecular Devices, LLC., CA, USA) and corrected for a 13 mV liquid junction potential.[167] Whole-cell patch-clamp recordings had to fulfill the following quality standards to be acceptable for analysis: spike amplitudes needed to be larger than 30 mV, the resting membrane potential had to be within a -48 mV to -80 mV range, the seal resistance before breaking into the cell needed to be larger than 6 GΩ, and at least one behavioral trial (walking or flight) meeting the criteria described below had to be recorded. In some experiments, e.g., in *ex-vivo* recordings, IPCs were depolarized via injection of a constant holding current to elicit spiking. Here, the above-mentioned quality standards for resting membrane potential and spike amplitude did not apply. Data were collected with a MultiClamp 700B amplifier (Molecular Devices, San Jose, CA, USA) in current clamp mode, low-pass filtered at 10 kHz and sampled (Digidata 1440A, Molecular Devices) at 20 kHz. If not explicitly stated, no holding current was injected throughout the experiments. The ability of IPCs to elicit post-inhibitory rebound responses was tested by injecting hyperpolarizing currents with of different amplitudes for 1 s (-50 pA, -75 pA, and -100 pA) and 15 s (-50 pA). The interstimulus interval was 60 s and the fly was tethered as shown in Figure 1A. Data were analyzed and figures were generated using custom-written MATLAB code (MATLAB 2020b, MathWorks, MA, USA). Subsequently, figures were further processed in Adobe Illustrator (Adobe, San Jose, CA, USA).

Tethered flight and walking

For the behavioral experiments shown in Figures 1, 2, 3E, 3F, 3H, 3I, 5A, 5B, and 5G, flight occurred either spontaneously or was induced by the application of gentle air puffs. Cessation of flight always occurred spontaneously. For flight analysis, we used a modified version of a wingbeat tachometer that detects wing motion via a light guide equipped with a long pass filter (760 nm and above, co-designed and built by the University of Cologne Animal Physiology Electronics Workshop, model 969), based on a design by IO Rodeo (https://github.com/iorodeo/light_sensor_boards). For the behavioral experiments shown in Figures 3, 4, and 5C–5G a setup functionally very similar to the one originally designed by Seelig and co-workers was used.[168,169] In brief, an air-supported ball (polypropylene, diameter: 6 mm, Spherotech GmbH, Fulda, Germany) was positioned under the fly using a 3D micromanipulator and a camera (acA1300-200um, Basler, Ahrensburg, Germany) providing a sideview for positional control. The spherical treadmill was illuminated via an 850 nm IR LED (SFH4550, OSRAM, Munich, Germany) and movement of the ball was recorded to calculate the trajectory of the walking fly (ball tracker).[169] For CsChrimson activation experiments, a 625 nm LED was adjusted to output ∼4.4 mW/cm^2 intensity at the position of the fly and was transiently switched on using pCLAMP.

Calcium imaging

For imaging experiments, the preparation followed the same protocol as for whole cell patch-clamp. However, the neural sheath was not ruptured and the calcium concentration in the saline was increased to match the composition commonly used (see for example Seelig and Jayaraman[170]) with a final concentration of: 103 mM NaCl, 3 mM KCl, 5 mM TES, 8 mM trehalose dihydrat, 10 mM glucose, 26 mM $NaHCO_3$, 1 mM NaH_2PO_4, 2.5 mM $CaCl_2$ dihydrat, 4 mM $MgCl_2$ hexahydrat. All calcium imaging data were recorded with a Prime BSI Express Scientific CMOS camera (Teledyne Photometrics, Tucson, AZ, USA) in an *in-vivo* fluorescence microscope (SliceScope, Scientifica). The image acquisition was controlled with the ImageJ based software Micro-Manager 2.0.[162] Time series data were acquired in a single z-plane at a framerate of 10 Hz for 2 min per trial. The field of view was adjusted to the respective position of the IPCs in each individual fly. The genetically encoded calcium indicator GCaMP6m was excited via a tunable LED (pE-4000 universal fluorescence illumination system, CoolLED Ltd., Andover, UK) set to 470 nm. The light beam was guided through a GFP filter set (Chroma, Bellow Falls, VT, USA) including a 495 nm long-pass filter and an excitation filter with a bandwidth of 450-490 nm. To eliminate nonspecific background light, an emission filter with a bandwidth of 500-550 nm was used before the emitted light was detected by the scientific CMOS sensor of the camera.

Immunohistochemistry and image acquisition

Flies were anesthetized on ice and fixed in ice-cold 4% paraformaldehyde in 0.1 M phosphate-buffered saline + 0.5% Triton-X100 (PBT, pH 7.2) for 3 h at RT on a rotarod. After a brief submersion in 70% ethanol, tissues of interest (brain only or the brain with attached VNC) were dissected in phosphate buffered saline (PBS) followed by three 15 min wash steps in PBT. Samples were pre-incubated overnight at 4°C in blocking solution (PBT containing 10% NGS) and then incubated in the following primary antisera: rabbit anti-DILP2 at a dilution of 1:2000 (RRID: AB_2569969, kindly provided by J. A. Veenstra, Bordeaux, France),[159] mouse anti-nc82 (Bruchpilot C-terminal aa 1227-1740) at a dilution of 1:50,[171] chicken anti-GFP (ab13970, abcam, Berlin, Germany) at a dilution of

1:1000. Next, samples were washed three times in PBT for 15 min, followed by incubation in secondary antibodies: AlexaFluor 488 (goat anti-chicken IgY (H+L), 1:200, Thermo Fisher Scientific, Waltham, MA, USA), AlexaFluor 555 (goat anti-rabbit IgG (H+L), 1:200, Thermo Fisher Scientific) and AlexaFluor 647 (goat anti-mouse IgG (H+L), 1:400, Thermo Fisher Scientific). Samples were, again, washed three times for 15 min in PBT and mounted in Vectashield Antifade Mounting Medium (H-1000, Vector Laboratories, CA, USA). Immunofluorescent labeling was visualized with a confocal laser scanning microscope (Leica TCS SP8 WLL) via Leica Application Suite X (LAS X, Leica Microsystems, Wetzlar, Germany) using HC PL APO 10×/0.4, HC PL APO 20×/0.75 IMM, or HC PL APO 63×/1.2 CORR objectives. Fluorophore signals were detected in serial stacks with a minimum resolution of 1024 × 1024 pixels using each dye's optimal laser line settings. Images were scanned sequentially to reduce dye cross-excitation. Image brightness and contrast were adjusted using LAS X.

QUANTIFICATION AND STATISTICAL ANALYSIS

All data analysis, except for the preprocessing of calcium imaging, was performed in MATLAB. Statistical tests used and p-values are described in Data S1 and the main text, the figures, or the figure captions. If not otherwise noted, values are presented as medians throughout the text and figure legends. Medians and interquartile ranges (IQR) are listed in Data S1.

IPC recordings were temporally smoothed using a running 2 ms window and thresholds were set manually in either the recording or the derivative of the recording to detect spikes. Accuracy of spike detection was confirmed for each experiment by manual inspection of three different sections of the recording (beginning, middle, and end). Spike frequency changes that occurred at behavioral transitions were analyzed in different intervals. For flight, these intervals were as follows: Each trial was divided into four 5 s intervals: before flight onset (pre), after flight onset (F1), before cessation of flight (F2), and after cessation of flight (post). The post interval started 500 ms after cessation of flight to account for the transition period. Since flight bouts had different lengths, mid-flight IPC activity is not depicted in the figures. For analysis of changes in membrane potential (V_m), intracellular recordings were filtered using a 100 ms wide running median filter, which was wide enough to eliminate the large membrane deflections during spikes. Here, the analysis window was 1 s before and after behavioral transitions. Flight trials were included for analysis if they featured at least 10 s of continuous flight in patch-clamp recordings and 8 s in calcium imaging experiments. The latter was chosen to match the shorter duration of calcium imaging trials we used to reduce bleaching and phototoxicity. In addition, trials of both methods were only included for further analysis if the inter-flight intervals were at least 15 s long. Flight onset and cessation were determined by extracting the time stamp of the first and last wingbeat in MATLAB for each flight bout. When calculating the average wingbeat frequency, we discounted the first and last 500 ms of each flight bout to exclude transition periods. In starvation experiments, IPC baseline activity was recorded for 8 min, from which only the last 5 min were analyzed.

Walking was determined by changes in translational velocity and thresholds for the detection of onset and cessation of walking were set manually in MATLAB. Only trials in which the fly was resting before onset and after cessation of a walking bout were considered for analysis. Within a 10 s window (5 s before onset and 5 s after cessation of walking) the fly was allowed to rotate the ball above threshold for a maximum of 500 ms. Locomotor trajectories reconstructed from treadmill rotations were individually inspected and sorted into two groups. In one group, only proper walking bouts characterized by relatively straight, uninterrupted walking trajectories were considered for analysis (45 % of all locomotor activity bouts), referred to as walking (Figures 3B and S2A). In the other group, all locomotor activity bouts, including those in which flies were turning on the spot, struggling on the spherical treadmill, or displaying unspecific leg movements inducing treadmill rotations were analyzed (238 bouts, referred to as locomotor activity, see Figure S2). For spontaneous walking and locomotor activity, bouts were accepted for analysis with a minimum duration of 5 s. Spike frequency was determined for each trial that was divided into four intervals: 5 s before walking onset (pre), 2 s after walking onset (W1/L1), 2 s before cessation of walking (W2/L2), and 5 s after cessation of walking (post). Since the walking bouts had different lengths, the mid-walking IPC activity is not depicted in the figures. For optogenetically induced backward walking via MDN activation, each trial was divided into four 5 s intervals: before LED onset (pre), after LED onset (MDN1), before LED cessation (MDN2), and after LED cessation (post). The LED stimulus duration was 15 s in all experiments. The post interval started 500 ms after cessation of backward walking to account for the transition period. To be considered for analysis, backward walking bouts had to meet the same criteria as spontaneous forward walking bouts (defined above). In *ex-vivo* preparations MDNs were activated for 5 s or 15 s. Each trial was divided into four intervals: 5 s before LED onset (pre), 2 s after LED onset (MDN1), 2 s before cessation of LED (MDN2), and 5 s after cessation of LED (post).

In PIR experiments, spike frequency was determined over 5 s before onset, 5 s after cessation, and during 1 s of hyperpolarizing current injections with different amplitudes (-50 pA, -75 pA, and -100 pA). During longer hyperpolarizations (15 s), only -50 pA was injected. Mean spike frequency was binned in these three intervals (binsize was 500 ms). For all three current injection levels, the median change in membrane potential was determined.

For calcium imaging, the motion correction of the raw video frames and the calculation of fluorescence changes was carried out using custom-written Python code that is part of the fly2p module (https://github.com/hjmh/fly2p). For preprocessing of the data, each frame was spatially filtered with a two-pixel-wide Gaussian filter and x/y motion corrected by using phase correlation to a reference image that was generated from the mean over 50 frames in the middle of the trial. Video S5 shows the motion corrected raw video corresponding to Video S2. To compute fluorescence changes as $\Delta F/F = (F-F_0)/F_0$, the fluorescence baseline F_0 was estimated by averaging over the 10% of lowest-intensity frames in each trial. $\Delta F/F$ was then calculated for each pixel over the whole time series. Next, individual IPC somata were manually delimited as regions of interest (ROIs) based on the reference image using the Napari

graphical user interface (https://doi.org/10.5281/zenodo.3555620). From these ROIs, mean ΔF/F time series values were extracted by averaging pixels within the ROI, and stored as csv files. Further population data analysis and Area under the curve (AUC) calculation was performed in MATLAB. To determine the AUC, the baseline (reference, 5 s) was subtracted from the ΔF/F values that were averaged over 5 s for onset and cessation of flight. The 2 s after the behavioral transition were accounted as a transition period and not included in our analysis (Figure 2D). For the probability distribution of ΔF/F, ΔF/F values during flight and after flight cessation were evaluated in 5 s long windows, excluding the first 2 s after the behavioral transition to account for the relatively slow indicator dynamics. The ΔF/F value from the resting state (baseline) were calculated from all remaining ΔF/F values of the recording during non-flight, excluding the 12 s after cessation of flight to account for the decay time of the calcium indicator.